Frequency- and temperature-dependent conductivity in $YBa_2Cu_3O_{6+x}$ crystals

Joseph Orenstein, G. A. Thomas, A. J. Millis, S. L. Cooper, D. H. Rapkine,
T. Timusk,* L. F. Schneemeyer, and J. V. Waszczak
AT&T Bell Laboratories, Murray Hill, New Jersey 07974
(Received 18 September 1989; revised manuscript received 24 April 1990)

The results of a systematic study of the optical properties of the $YBa_2Cu_3O_{6+x}$-based insulators and superconductors are reported. Specifically, we present measurements and analysis of the optical reflectivity R of a series of $YBa_2Cu_3O_{6+x}$ crystals in the frequency range from 30 to 20 000 cm^{-1} (4 meV to 2.5 eV), and temperature range from 10 to 270 K. From R we obtain the real part of the frequency-dependent optical conductivity $\sigma(\omega)$ by Kramers-Kronig analysis. In our discussion, we emphasize the development of structure and spectral weight in $\sigma(\omega)$ as the compounds change from insulators to high-T_c superconductors with varying O content or Al doping. We identify the free carrier, and interband components of $\sigma(\omega)$, and focus on the free-carrier component. The free-carrier component is analyzed by calculating $\sigma(\omega,T)$ within a model in which carriers scatter from a spectrum of dispersionless oscillators parametrized by $\alpha^2F(\omega)$ (where α is the coupling constant and $F(\omega)$ is the density of modes). For $\omega<50$ meV, $\sigma(\omega,T)$ is well described by weak coupling ($\lambda\simeq0.4$) to an $F(\omega)$ which is broad on the scale of k_BT. From the fit we obtain the inelastic scattering rate as a function of T, and the spectral weight in the translational, or Drude mode, of the quasiparticles. Above 50 meV, σ cannot be fit by this scattering model, with any $\alpha^2F(\omega)$, which suggests a two-component picture of $\sigma(\omega,T)$. As T is lowered, a "knee" in $R(\omega)$, and a threshold in the corresponding $\sigma(\omega)$, is resolved, which we associate with the low-frequency edge of this second component. In addition, a second threshold in the range 15–20 meV is seen at low T, although the magnitude of the change in R is close to our detection limit of 1%. We compare the properties of these thresholds with expectations for a superconducting energy gap as described in BCS theory. Finally, we discuss the implications of other experiments, which also probe the spectrum of low-energy excitations in the cuprate superconductors, on the interpretation of $\sigma(\omega,T)$.

I. INTRODUCTION

The frequency- and temperature-dependent optical reflectivity $R(\omega,T)$ is a powerful probe of a system of interacting electrons. In this paper, we report measurements of $R(\omega,T)$ in a series of $YBa_2Cu_3O_{6+x}$ crystals with different compositions which range from insulator to high-T_c superconductor. From R we obtain the real part of the conductivity, $\sigma(\omega,T)$, by Kramers-Kronig (KK) analysis. In this section we introduce the two main motivations for this work: the direct connection between $\sigma(\omega,T)$ in the cuprate superconductors and the low-energy excitations which scatter the charge carriers, and the importance of studying the high-T_c cuprates as a function of the concentration of free carriers.

A. Optical conductivity as a probe of charge-carrier dynamics

The optical conductivity measures the rate at which particle-hole pairs are created by photons of frequency ω. In a translationally invariant system, light couples only to pairs with nearly zero momentum (on the scale of the Fermi momentum) and the allowed excitations have $\omega=0$. The conductivity is proportional to $\delta(0)$, the Dirac δ function centered at $\omega=0$, reflecting the perfect conductivity of a system without scattering. In real metals, however, σ acquires a nonzero width from the breakdown of translational invariance enforced by disorder in the lattice and by the presence of a surface.[1] In the cuprate superconductors, the lattice dominates, and the magnitude and frequency dependence of σ reflects the scattering of carriers in the bulk.

To see how this comes about, we describe the effect of the lattice and the surface on σ. As described by Bloch's theorem, carriers are not scattered by a perfect lattice and the low-frequency contribution to σ remains proportional to $\delta(0)$. Disorder in the lattice potential, either static or dynamic, restores width to σ because it allows photons to couple to particle-hole pairs with nonzero center-of-mass momentum. Static disorder broadens the δ function to a Lorentzian, of width equal to the scattering rate, v_F/l, where v_F is the Fermi velocity and l is the mean free path. Dynamic disorder, which arises from fluctuations in the periodic charge and spin density, introduces a different frequency dependence to σ. Without static disorder and at nonzero temperature, the width of σ reflects the T-dependent inelastic mean free path; at $T=0$ the δ function at $\omega=0$ is restored, but an additional component of σ remains in a range of frequencies which reflects the spectral density of the fluctuations.[2]

For metals in which l is large, the effect of the surface can dominate bulk scattering, and make the intrinsic dynamics more difficult to measure. Because of the surface, the external electric field E is not uniform in space and decays exponentially with distance from the surface, de-

creasing by $1/e$ in a "skin depth" δ. If $l > \delta$, then the broadening due to interaction with the surface will dominate the effect of carrier scattering in the bulk.[1]

As we will see later, the $YBa_2Cu_3O_{6+x}$ superconductors are characterized by $\delta \sim 10^3$ Å, and l (at 100 K) $\sim 10^2$ Å, so that $\sigma(\omega)$ is dominated by bulk effects. In addition, the reasonably large value of δ means that infrared reflectivity is not as surface sensitive as other low-energy spectroscopies, such as tunneling and photoemission. As a result, $\sigma(\omega, T)$ is an important probe of both the static disorder and the low-frequency excitations which scatter carriers in the high-T_c cuprate superconductors.

B. Importance of varying carrier concentration

Our second main motivation is to measure the evolution of a key property of the high-T_c compounds as a function of the concentration of free carriers. One of the fascinating aspects of the cuprates is that the superconducting phase is near an antiferromagnetic (AF) insulating phase which arises from the effects of Coulomb interactions in a half-filled band. Bednorz and Müller[3] discovered that a high-T_c phase appears when electrons are removed from the AF (CuO_2) planes. Some physical properties, such as the Hall resistance[4,5] and conductivity,[6] suggest that the carrier density increases continuously as more electrons are removed, in a manner which is analogous to acceptor doping of a conventional insulator. The theoretical description of the spin, interactions, and even the quantum statistics of charge carriers in this metallic phase is at an early stage, and there are suggestions that the proximity to the insulator is central to the mechanism for high-T_c superconductivity.[7] To test these ideas it is important to study the physical properties of these materials through, and beyond, the insulator-to-metal transition.

In the following sections of this paper, we report the results of a systematic study of the optical properties of the $YBa_2Cu_3O_{6+x}$-based insulators and superconductors. In Sec. II A, we discuss the details of the sample preparation, and characterization by techniques other than optical reflectivity. Section II B contains a description of the reflectivity apparatus, and the details of the KK analysis. Two main quantities determined from this analysis, $\sigma(\omega, T)$, and the effective carrier number per call, $N_{\text{eff}}(\omega, T)$, are presented in Sec. III. Section IV contains a detailed discussion of $\sigma(\omega, T)$ in the normal and superconducting state. This discussion is summarized, with emphasis on the main conclusions, in Sec. V.

II. EXPERIMENT

A. Sample preparation and characterization

The measurements reported in this work were performed on samples each composed of one crystal of $YBa_2Cu_3O_{6+x}$, with typical dimensions $2 \times 2 \times 0.1$ mm^3. The crystals are prepared in two stages.[8] In the first stage, a partial melt of rare-earth oxide, barium carbonate, and copper oxide are cooled to room temperature in a zirconia crucible to produce nearly free-standing crystalline platelets. The platelets, which are microtwinned in the a-b plane, are pinned in a few places to the underlying flux. Removal of the crystals is accomplished through the use of a commercial dentist drill. These "as-grown" crystals are bulk superconductors (as determined from the magnitude of the Meissner effect), but have broad resistive transitions with midpoints ≈ 50 K, as is characteristic of samples in which the O content is inhomogeneous and $x \approx 0.5$. In the second stage of sample preparation, the crystals are annealed in O_2 to increase the homogeneity of the value of x. The crystals must be annealed for much longer periods of time than ceramic samples in order to achieve a comparable degree of homogeneity. We annealed our crystals for several weeks, which is the time scale for O diffusion suggested by measurements of electrical resistivity during exposure to O_2 at elevated temperatures.[9]

Several dozen crystals prepared in this manner were screened on the basis of their room-temperature reflectivity in the mid infrared. Those with the highest R were selected for an additional screening by measurement of far-infrared reflectivity in the superconducting state.[10] Finally, samples which had R consistent with unity in the superconducting state were chosen for measurement of $R(\omega, T)$ in the frequency, and temperature range of 30–20 000 cm^{-1} and 10–270 K, respectively.

From the superconducting samples with the largest R, we chose to focus in this paper on four samples which best illustrate the variation in optical properties as a function of proximity to the insulating phase. For comparison, we have also included optical spectra of an insulating sample which was prepared by annealing in N_2 after the growth stage. The four metallic samples have resistive and susceptibility transitions at 30, 50, 80, and 90 K. The samples with the three highest values of T_c were annealed at 600 , 550 , and 450 °C, respectively. The fourth sample was prepared in an alumina crucible (which leads to a replacement[11] of $\sim 10\%$ of the chain Cu atoms by Al) and were annealed at 600 °C.

Additional characterization was performed on samples from the same batches as those studied optically. The most extensive characterization has been of the samples with the highest T_c. These crystals have resistive transitions with widths less than 1 K.[9,10] Their magnetic response is consistent with perfect diamagnetism and full Meissner effect (although the absolute uncertainty is $\sim 30\%$ because of the shape).[12] In addition, these crystals show high surface conductance,[13] sharp superconducting onsets in microwave absorption,[14] instrumentally limited channeling ($\chi_{\text{min}} = 3$–5%) in Rutherford backscattering,[15] and unmeasurably small c-axis misalignment in x-ray scattering[16] and electron diffraction.[17]

The samples with lower-T_c values have been characterized by the same techniques. The resistive transitions of the lower-T_c samples are broader,[10] as expected if the O distribution in the O-Cu-O chains is disordered. The measurements of diamagnetism, Meissner effect, and crystallographic alignment are similar to the higher-T_c samples. Of particular interest is the absence of evidence for regions with $T_c = 90$ K in the conductivity,[10] suscepti-

bility,[12] or microwave absorption[18] of the low-T_c samples.

A summary of these characterization measurements is presented in Figs. 1–3. These contain plots of resistivity (ρ), static magnetic susceptibility (χ), and the loss component of the ac magnetic susceptibility (χ'') as a function of T, respectively. The measurements of $\chi(T)$ were performed on the same five crystals as studied optically. The other measurements, which involve surface damage, were performed on samples from the same batches as the crystals which were used for the optical experiments. For these measurements we present data on samples with $T_c \simeq 60$ and 90 K.

The resistivity of two representative crystals is presented in Fig. 1. For the 90-K crystal, shown in Fig. 1(a), $d\rho/dT = 0.47$ $\mu\Omega$ cm/K, $\rho(T_c) = 50$ $\mu\Omega$ cm, and $\rho_0 = 10$ $\mu\Omega$ cm, where ρ_0 is the extrapolation of a linear fit to $\rho(T)$ to $T = 0$. All of these values are consistent with the published reports of lowest resistivity $YBa_2Cu_3O_{6+x}$ crystals. For the crystal with $T_c \simeq 60$ K, shown in Fig. 1(b), the corresponding values are $d\rho/dT = 1.3$ $\mu\Omega$ cm/K, $\rho(T_c) = 240$ $\mu\Omega$ cm, and $\rho_0 = 100$ $\mu\Omega$ cm. Results for two additional crystals are shown in Figs. 1(c)

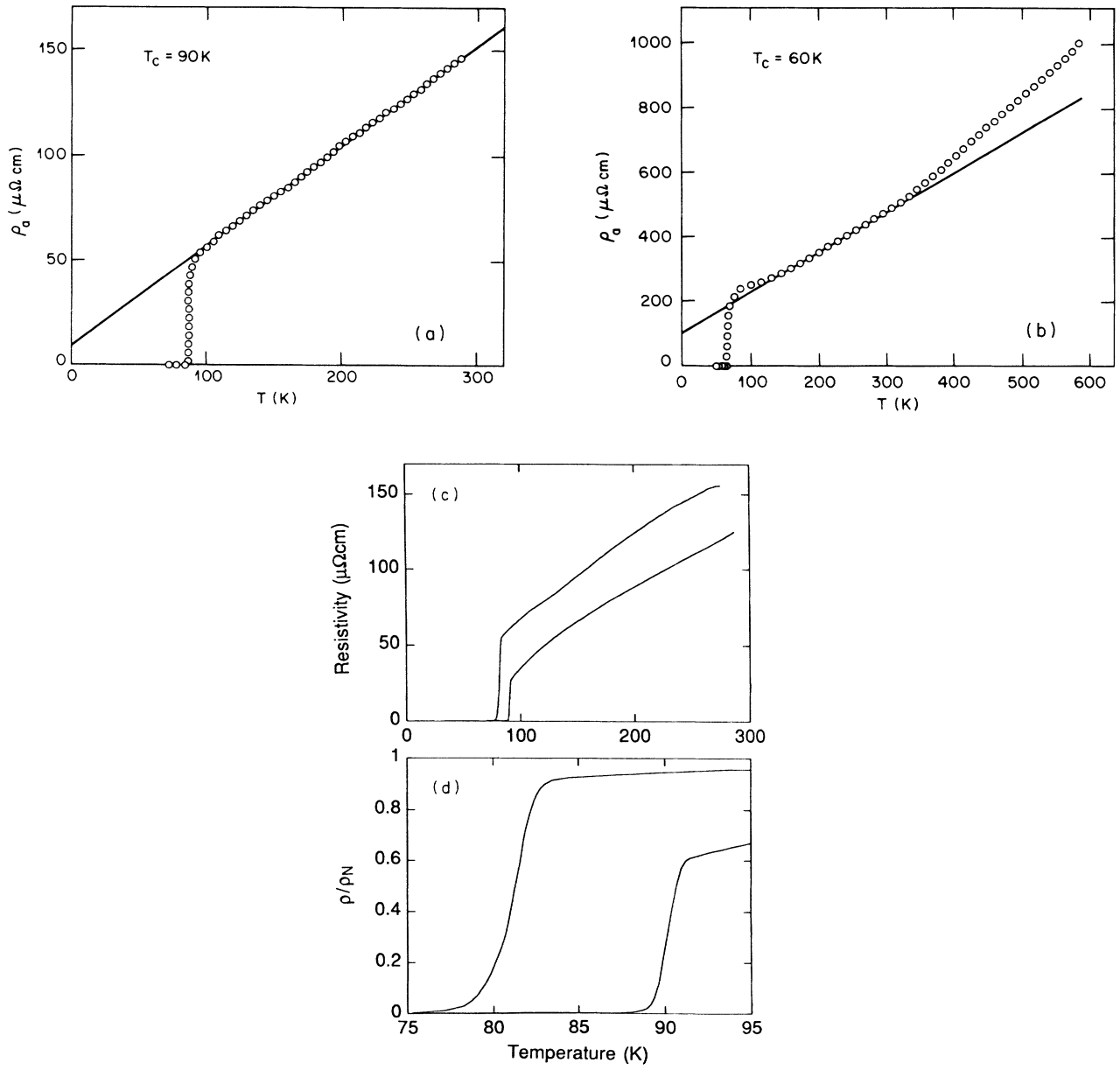

FIG. 1. Resistivity in the a-b plane at $\omega = 0$, ρ_a, or ρ, as a function of temperature T, for four crystals from the same preparations as those shown in subsequent figures. (a) Sample with $T_c = 90$ K, with linear fit for comparison, (b) sample with $T_c = 60$ K with similar fit over a wider T range, (c) two samples with $T_c = 80$ and 90 K, (d) expanded view of the region near T_c for the same samples. These crystals illustrate criteria used to select material for optical measurements in that the transitions are narrow in T and the resistivities are low. Further discussions presented in Refs. 8–10.

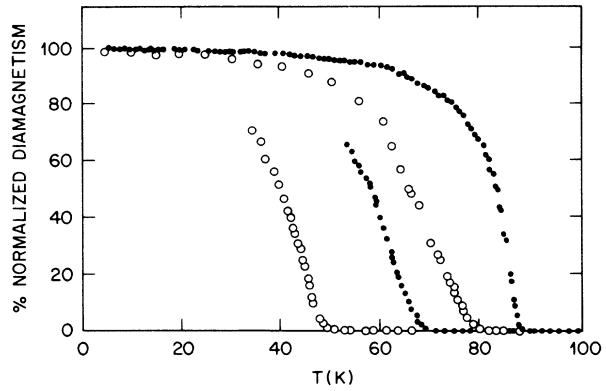

FIG. 2. Diamagnetism normalized to its low-T value as a function of T for four representative crystals from Ref. 12. The absolute values in the low-T limit are consistent with full diamagnetic screening, and no indication is seen of more than one superconducting transition in any crystal selected for study. The crystals whose diamagnetism is shown, with T_c values 90, 80, 70, and 50, were all studied optically with the results either presented below or in Ref. 22.

and 1(d), and have been discussed in Ref. 10.

Static magnetic susceptibility is presented in Fig. 2. The measurements were performed in a commercial SQUID magnetometer in a field of 5 Oe. In order to compare the transitions, the curves were scaled to the same low-temperature value of χ. For all of the crystals the magnitude of the diamagnetic susceptibility is consistent with bulk superconductivity, although χ is well known not to be a reliable quantitative measurement of the volume fraction of superconducting material. In agreement with earlier work on ceramic samples, the transitions are sharpest for values of T_c near 60 and 90 K, and broaden dramatically at other T_c's.

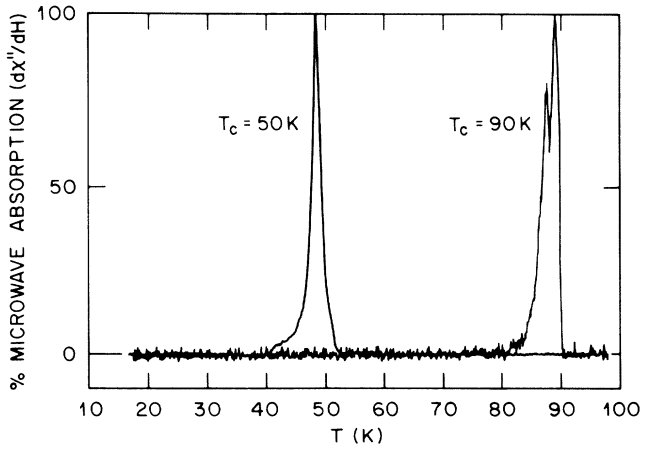

FIG. 3. Percent microwave absorption as function of T for two crystals with $T_c = 50$ and 90 K, similar to those measured optically. The measurement technique is discussed in Ref. 14. The results show that crystals with reduced T_c can have transitions as narrow as those with T_c near 90 K, and can show, with high sensitivity, no indication of the presence of material with another T_c, e.g., a 90-K T_c.

Perhaps the most useful characterization for the subsequent interpretation of our optical data are the measurements of energy dissipation at microwave frequencies presented in Fig. 3. The loss measurements are performed in a standard X-band cavity, with the sample positioned at a node in the electric field. The derivative of χ'' with respect to magnetic field is measured by synchronous detection of the change in cavity reflectivity induced by a field modulation coil. The value of the static field is ≈ 100 G. The sensitivity of χ'' to H results from the appearance of shielding currents at the onset of the superconductivity. Unlike resistivity measurements, which are shorted by the highest-T_c percolating phase, the microwave loss is sensitive to all minority superconducting phases. Figure 3 shows data for crystals with T_c of 60 and 90 K. These traces show that the concentration of the 90-K phase in the 60-K material, and vice versa, is undetectably small.

B. Experimental methods

1. Apparatus

The experiments were carried out using two separate Fourier-transform spectrometers. For the far-infrared measurements (~ 30–700 cm^{-1}), the interferogram was acquired with the step and integrate procedure. Light from the Hg source reached the detector by passing through light pipes and reflecting from either the sample or Au reference mirror. The sample and Au reference were interchanged in the beam path by a manipulator operated externally to the sample chamber. R spectra at higher frequencies (~ 500–$20\,000$ cm^{-1}) were measured with a rapid-scanning interferometer. The modulated, collimated light beam from the spectrometer was focused on the sample with mirror optics, and the reflected beam was refocused on one of a set of detectors (each optimized for different frequency ranges with substantial overlap). The sample and reference were interchanged by moving the cryostat, which was supported by an xyz translation stage. In both experimental setups, the diameter of the light beam at the sample position was ~ 1.75 mm, and the angle of incidence was $\sim 10°$.

2. References and absolute uncertainties

Uncertainties arise in our measurements of the absolute reflectivity because of the need to compare the sample and a reference. The references were made of thick Au films evaporated with a Cr underlayer on optically polished sapphire substrates. We find these opaque mirrors to be measurably higher in reflectance than polished brass or other metals tested, even in the far infrared, and we find negligible variation among Au references.

The absolute uncertainly, which we estimate to be 1%, comes partly from the Au reflectivity. To estimate $R(\omega, T)$ for our Au mirrors in the far infrared, we measured the dc conductivity as a function of temperature, and used literature values[19] for the carrier density (5.9×10^{22} cm^{-3}) and effective mass ($m^*/m \simeq 1$) to obtain the free-carrier scattering rate $\Gamma(T)$. We then calcu-

lated $R(\omega,T)$ by assuming a Drude form for the conductivity,

$$\sigma(\omega,T)=\sigma(0)/[1+(\omega/\Gamma)^2] .$$

At room temperature, $\sigma(0)=40\,000\ \Omega^{-1}\,\mathrm{cm}^{-1}$, which corresponds to $\Gamma=240\mathrm{cm}^{-1}$. The calculated R decreases from 1.0 at $\omega=0$ to 0.995 at $\omega\simeq\Gamma$, and gradually decreases to 0.99 at $\omega=20\,000\ \mathrm{cm}^{-1}$. At $T=100$ K, $\sigma(0)$ increases by a factor ~ 4, and $R(\omega)$ is ~ 4 times closer to unity over the entire frequency range.

An uncertainly of comparable size comes from the difficulty in establishing precise optical alignment as the sample and reference are interchanged. This error shows up in the comparison of spectra measured with the two spectrometers in the frequency range in which they overlap. These overlapping segments are shifted as needed (by 1% or less) to form a complete, smooth curve.

3. *Kramers-Kronig transformations*

We have calculated the real and imaginary parts of σ by performing Kramers-Kronig transformations of the measured R. Since the transformation requires σ for $0<\omega<\infty$, assumptions must be made in order to extrapolate beyond the upper and lower bounds of the measurement, ω_U, and ω_L, respectively. For $\omega>\omega_U$, we have assumed[20]

$$R=R_\infty+(R_U-R_\infty)\omega_U^4/\omega^4 ,$$

where R_U is the reflectivity at ω_U, and R_∞ is the value in the $\omega\rightarrow\infty$ limit obtained from other measurements[21] at large ω. Because R is relatively featureless at frequencies near the upper range of our measurement, we believe that the KK analysis below ~ 1 eV is not sensitive to the extrapolation.

For $\omega<\omega_L$ we have used different interpolations between the lowest measured frequency ω_L and $\omega=0$ (where R must equal 1.0), for the superconducting and normal states. In the normal state, we set

$$R=1-(1-R_L)\left[\frac{\omega}{\omega_L}\right]^{1/2} ,$$

where R_L is the reflectivity at ω_L. This frequency dependence is the Hagen-Rubens (HR) approximation to R of metals, which is accurate when $\omega\ll\Gamma$.[20] As we will see, in the $YBa_2Cu_3O_{6+x}$ metallic compounds, $\Gamma\approx 2k_BT$, so that the HR approximation should be reasonably accurate for $\omega<140\ \mathrm{cm}^{-1}$ (at $T=100$ K), which is well above $\omega_L\simeq 30\ \mathrm{cm}^{-1}$. In addition, we have tested other interpolations below ω_L, such as a straight line from ω_L, R_L to $\omega=0$, $R=1.0$, and we find no significant difference in the resulting conductivity for $\omega>\omega_L$.

In the superconducting state, the samples we have analyzed have a nearly constant R with a value consistent with unity at low frequencies. For the KK transformations we have set $R=1$ in this region, as is expected for the reflectivity of a superconductor with no states in the gap. Other extrapolations, in which R goes to unity (and σ to zero) smoothly as ω approaches zero, cannot be ruled out, given the $\sim 1\%$ experimental uncertainty. In Sec. IV D 1 we describe in more detail the range of $\sigma(\omega)$ consistent with the possible errors in R at low ω.

III. RESULTS

A. Definition of $N_{\mathrm{eff}}(\omega,T)$

In this section we present the reflectivity spectra and the model-independent information which can be obtained directly by KK analysis of R. We emphasize two important spectral functions, the real part of the conductivity $\sigma(\omega,T)$ and a dimensionless measure of spectral weight $N_{\mathrm{eff}}(\omega,T)$. N_{eff} is defined according to the relation

$$N_{\mathrm{eff}}(\omega)\equiv\frac{2mV_{\mathrm{cell}}}{\pi e^2}\int_0^\omega\sigma(\omega')d\omega' , \tag{1}$$

where e and m are the bare electronic charge and mass, respectively, and V_{cell} is the unit-cell volume.

The significance of $N_{\mathrm{eff}}(\omega)$ may be appreciated by considering the sum rule on the conductivity

$$\int_0^\infty\sigma d\omega=\frac{\pi ne^2}{2m}\equiv\omega_p^2/8 , \tag{2}$$

where n is the total density of electrons.[20] For the translationally invariant system described in the Introduction,

$$\sigma(\omega)=\frac{\pi ne^2}{m}\delta(0) .$$

Interband transitions, which are introduced by the lattice, remove spectral weight from the δ function, and transfer it to large frequencies characteristic of bandgaps in the solid. The change in spectral weight at low frequency is usually expressed by replacing the total number density of electrons by the density in the conduction band, and by renormalizing the carrier mass from m to an optical or band mass, m_0. If the integral in Eq. (1) is cut off (at ω_g) so as to include only the intraband contribution to σ (the δ function at $\omega=0$ broadened by disorder), then

$$N_{\mathrm{eff}}(\omega_g)=\frac{nV_{\mathrm{cell}}}{m_0/m} ,$$

which is simply the number of free carriers per unit cell if $m_0/m=1$. In general, $N_{\mathrm{eff}}(\omega)(m_0/m)$ is equal to the number of carriers which contribute to the conductivity below a frequency ω.

B. Spectra of R, σ, and N_{eff}

Figure 4 shows R, measured at 100 K, for four crystals of different T_c. Previously, it has been shown in crystals[22] and in ceramics[23] that R in the $YBa_2Cu_3O_{6+x}$ family of compounds is extremely sensitive to the concentration of O. What is notable about this series of crystals is that they show high values of R for $\omega\lesssim 450\ \mathrm{cm}^{-1}$ in the normal state, and R consistent with unity for $\omega\lesssim 100\ \mathrm{cm}^{-1}$ in the superconducting state. Nevertheless, the spectra show enormous variation in R for frequencies greater than $\sim 500\ \mathrm{cm}^{-1}$.

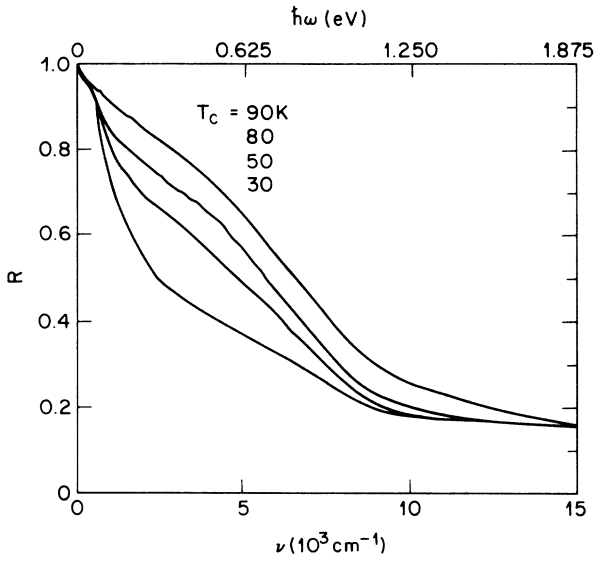

FIG. 4. Reflectivity R as a function of frequency ω (lower scale) and energy $\hbar\omega$ (upper scale) for four crystals of $YBa_2Cu_3O_{6+x}$ whose values of the superconducting transition temperature T_c are indicated. The three higher T_c samples were produced by changing the O concentration, while that with $T_c = 30$ K has both controlled O and Al doping. The light is unpolarized with the incident electric field $\simeq 12°$ from the a-b plane of the microtwinned crystals which are held at $T = 100$ K.

The spectra of σ, derived from a KK analysis of the R spectra in Fig. 4, are plotted in Fig. 5. Also shown is a previously published spectrum of a crystal with even lower oxygen content, $x \sim 0.2$, which does not have metallic conductivity or a superconducting transition. The

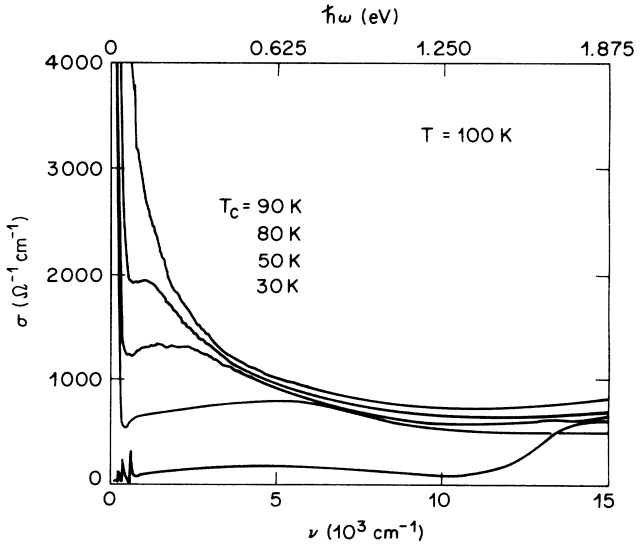

FIG. 5. Electrical conductivity σ as a function of frequency (and energy) for the same crystals as in Fig. 4, and, in addition, for an insulating crystal with an O concentration corresponding to $x \sim 0.2$ (lowest curve). These curves are obtained from a Kramers-Kronig transformation of the data in Fig. 4 and represent the behavior in the a-b plane. The curves have been smoothed, and some phonon structure in the metallic samples has been removed. (The phonons are shown for the insulator.)

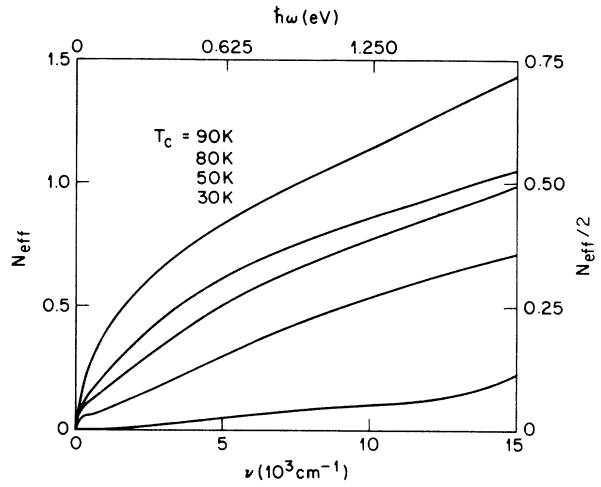

FIG. 6. The dimensionless spectral weight N_{eff} *per unit cell* (left scale), and *per plane Cu* (right scale), as a function of frequency (and energy). The data are obtained by integrating the area under the curves for σ for the same five crystals as in Fig. 5.

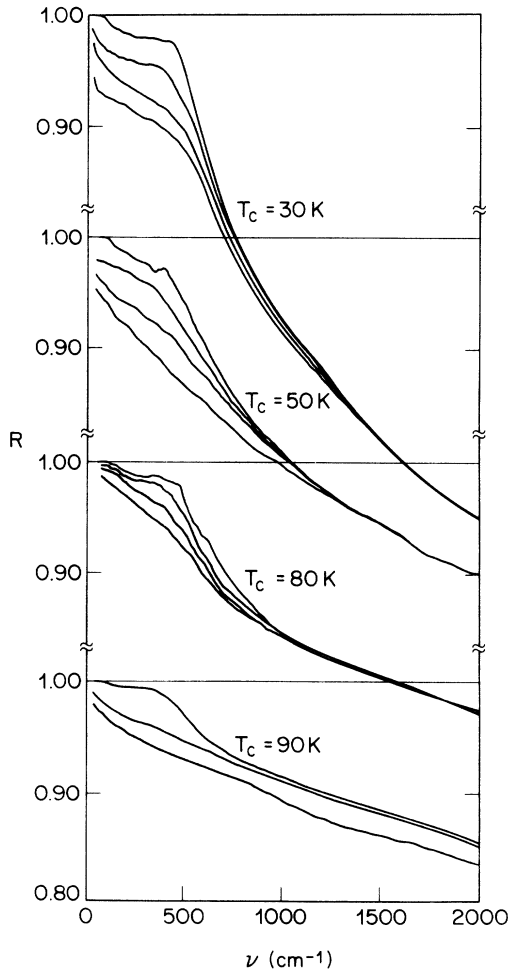

FIG. 7. Reflectivity as a function of frequency for the same four crystals as in Fig. 4 with each of the samples held at various temperatures, as follows: (T_c: T)=(30 K: 10, 100, 150, 250 K), (50 K: 10, 100, 150, 250 K), (80 K: 10, 40, 80, 150 K), (90 K: 20, 100, 200). Curves were smoothed as described above.

spectra are plotted on an expanded vertical scale, which shows the mid-infrared region most clearly. (σ at low ω is shown for each sample in Fig. 8.) Figure 6 shows N_{eff} for each sample, obtained by integration of the spectra in Fig. 5. Using Eqs. (1) and (2), N_{eff} can be converted to an equivalent plasma frequency through the relation

$$\omega_p^2 \text{ eV}^2 = \frac{4\pi e^2}{m}\frac{N_{\text{eff}}}{V_{\text{cell}}} = 7.95 N_{\text{eff}} .$$

The scale on the right-hand side of Fig. 6 is $N_{\text{eff}}/2$, which reflects the effective number of carriers per Cu(2) site, rather than per cell.

In Figs. 7–9, we illustrate the temperature dependence of $R(\omega)$, $\sigma(\omega)$, and $N_{\text{eff}}(\omega)$, respectively, for the same series of metallic samples. The expanded scale in Fig. 7 highlights the low-frequency behavior of $R(\omega,T)$. In each panel, the curve with the highest R was measured in the superconducting phase ($T=10$ K for the crystal with $T_c=80$ K and $T=20$ K for the others). The temperatures at which the other spectra were measured are indicated in the caption. The curves of $\sigma(\omega)$ which correspond to the R spectra of Fig. 7 are shown in Figs. 8(a)–8(d). $N_{\text{eff}}(\omega,T)$, obtained by numerical integration of $\sigma(\omega,T)$ in Figs. 8(a)–8(d), is plotted as a function of ω in Fig. 9. The normal-state N_{eff} curves (for the same sample) come together above ~ 6000 cm^{-1}. This shows that, as T is reduced, the spectral weight shifts to lower frequency but the total weight does not change below 6000 cm^{-1}, as expected on the basis of the f sum rule [Eq. (2)]. Confirmation of the f sum rule provides a useful check on the validity of our reflectivity measurements and the subsequent analysis. The N_{eff} curves for the superconducting state show a reduction of spectral weight compared to the normal state for each of the samples. The "missing area" in the curves of σ in the supercon-

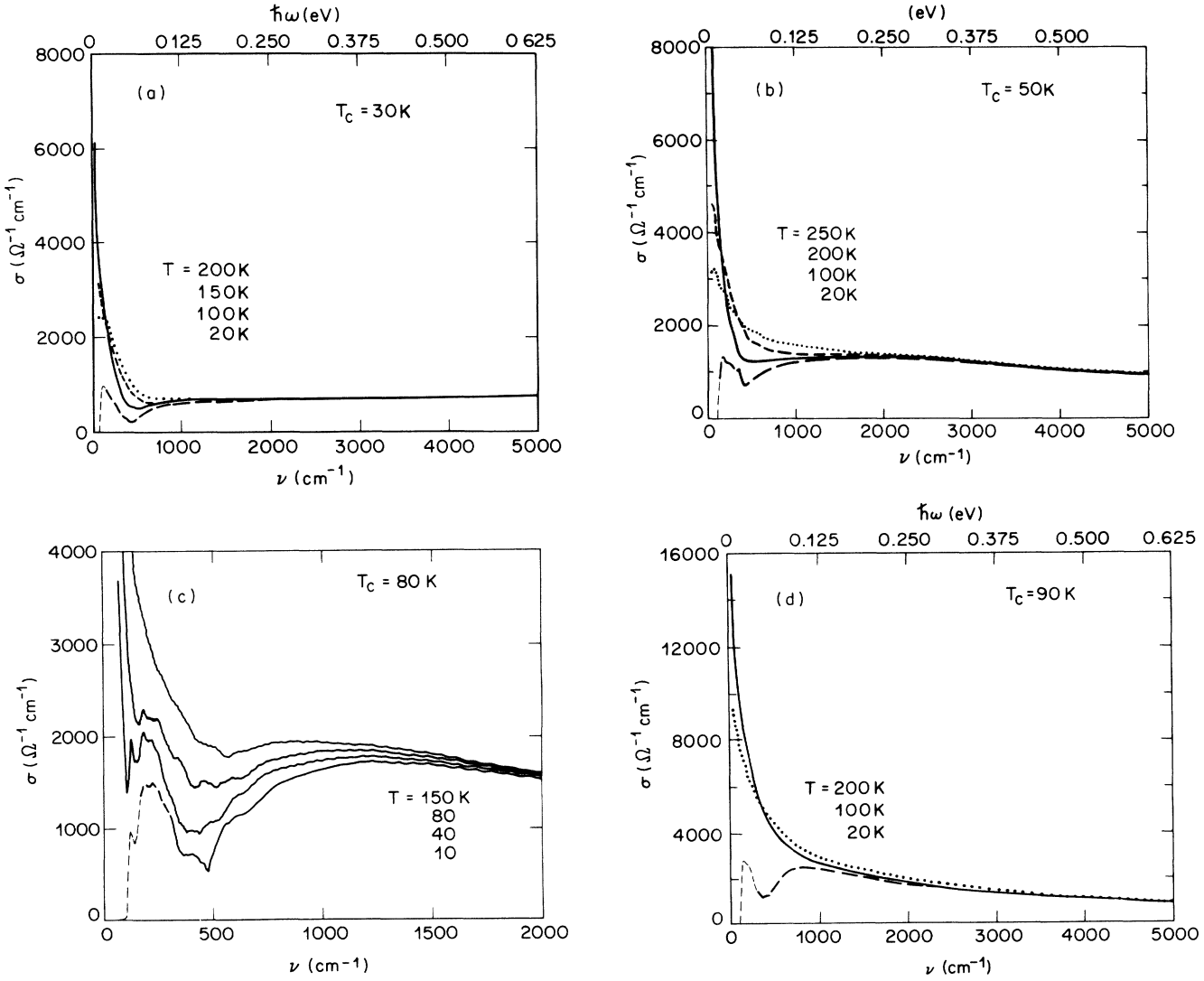

FIG. 8. Four-part figure showing the conductivity σ as a function of frequency (and energy) derived from the reflectivity data of Fig. 7 using Kramers-Kronig transformations. Different curves shown are for different temperatures, as labeled. (a)–(d) show data for the crystals with T_c values as labeled (30, 50, 80, 90 K). The lightly dashed part of the curves in the superconducting state indicate data with large uncertainty (as illustrated in Fig. 14) because the reflectivities closely approach 1.

ducting state appears in a δ function at $\omega=0$, and this contribution is not included in the numerical integration which yields $N_{\rm eff}(\omega)$. The difference between $N_{\rm eff}$ in the normal and superconducting states is a measure of the strength of the δ function, and is proportional to the spectral weight in the superfluid condensate.[24]

IV. ANALYSIS

In this section we analyze the results presented in Sec. III. In Secs. IV A and IV B we focus on the spectra in Fig. 5, which show the change in $\sigma(\omega,100\ {\rm K})$ as $YBa_2Cu_3O_{6+x}$ evolves from insulator to high-T_c metal with increasing O concentration. The spectrum of the insulating sample is described in Sec. IV A. In Sec. IV B the metallic spectra are analyzed, with emphasis on the identification of the free carrier and the interband contributions to σ. In Sec. IV C we study in detail the temperature and frequency dependence of σ. In particular, we calculate $\sigma(\omega,T)$ for a model in which free carriers scatter from a spectrum of dispersionless oscillators, and compare the theoretical curves with the experimental data. Finally, in Sec. IV D we describe the features in σ which emerge as the metallic samples are cooled below T_c, and discuss their interpretation as energy gaps in the superconducting state.

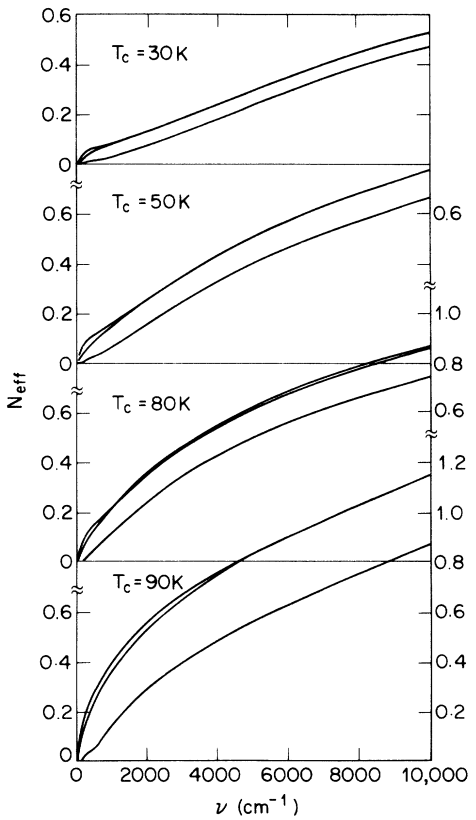

FIG. 9. Dimensionless spectral weight per unit cell as a function of cutoff frequency ν. The curves are obtained from integrating some of the conductivity curves of Fig. 8 up to the cutoff. The four parts of the figure are for the crystals with T_c values as indicated. The different curves for each are for different temperatures (top to bottom): (T_c: T)=(30 K: 100, 200, 20 K), (50 K: 100, 200, 20 K), (80 K: 150, 80, 10 K), (90 K: 100, 200, 20 K). As T is lowered, the spectral weight first shifts to lower, but nonzero frequency. In the superconducting state $N_{\rm eff}$ is smaller overall, reflecting the shift of spectral weight in a δ function at $\omega=0$ which is not included in the numerical integration. The difference in $N_{\rm eff}$ in the normal and superconducting states is a measure of the spectral weight in the superfluid condensate.

A. Insulating phase

1. Introduction

Confirming early suggestions,[25] a wide variety of spectroscopic measurements[26] and quantum chemical and density-functional theory calculations have indicated that, in La_2CuO_4 and $YBa_2Cu_3O_6$, the CuO_2 planes are charge-transfer insulators.[27–30] These results suggest that, in the charge state Cu^{2+}-O^{2-}, there is one hole per CuO_2 complex, which resides mainly on the Cu site. The charge-transfer energy ε_p-$\varepsilon_d\sim 2$–3 eV inhibits hopping of the hole from a Cu to an O site, and a large correlation energy, $U_{dd}\sim 8$–10 eV, prevents occupancy of a Cu site by a second hole. If ε_p-ε_d is sufficiently large compared to the Cu-O transfer integral [as is apparently the case in La_2CuO_4 and $YBa_2Cu_3O_6$ where $t_{\rm Cu\text{-}O}\sim 1.5$ eV (Refs. 31 and 32)], the material will be an insulator. The threshold for optical excitation, which occurs at an energy E_{xt} of order ε_p-ε_d, corresponds to a transition in which a hole moves from a Cu d site to an O p site.

2. Conductivity in the insulating phase

The conductivity of the insulating sample is shown in Fig. 5. The spectrum is consistent with a wide-band insulator, with a bandgap ≈ 1.75 eV. In particular, there is no free-carrier peak near $\omega=0$, and the relatively small contribution to $\sigma(\omega)$ from optic phonons dominates at low frequency. The onset of absorption near 1.75 eV was also observed by Tajima *et al.*[21] in their recently reported study of σ up to $\omega=15$ eV. They found that, above this onset, σ is relatively flat until additional transitions set in at $\omega\simeq 4$ eV. The spectral weight in the frequency range $1.75<\omega<4$ eV is comparable to that predicted to be at $\omega=0$ by band-structure calculations (which find a metallic ground state for the CuO_2 planes).

Below the absorption edge at 1.75 eV there is a broad contribution to σ which peaks at ≈ 0.5 eV, which we believe is not intrinsic to the CuO_2 layers in the Cu^{2+}-O^{2-} state. The evidence for this is twofold: the absorption in this frequency range is small and it varies in magnitude among different insulators. As Fig. 6 shows, the spectral weight below the onset of interband absorption at 1.75 eV corresponds to an $N_{\rm eff}$ [per Cu(2) site] of only ≈ 0.06. In samples of Eu_2CuO_4, which contains CuO_2 layers essentially the same structure as $YBa_2Cu_3O_{6+x}$ and La_2CuO_4, the spectral weight below the absorption threshold at 1.75 eV is a factor ≈ 10 smaller than in the insulating sample in Fig. 5, or in samples of La_2CuO_4 that we have

studied.[33] This small weight is consistent with the observation that Eu_2CuO_4 is more resistant to acceptor doping than the other materials.[34] Overall, the spectroscopic evidence supports the idea that the CuO_2 layers in the state Cu^{2+}-O^{2-} are insulators with a charge-transfer gap of ≈ 1.75 eV.

B. Metallic phase

1. Introduction

In principle, when δ electrons per site are removed from the CuO_2 planes by varying the electronegativity of adjacent atomic layers (for example, by changing their O content), we expect the onset of metallic conduction. In reality, the compensating negative charge on adjacent layers is not uniformly distributed; instead it is located at lattice sites which will bind carriers at low densities. The critical value of δ at which the metal-insulator transition takes place will reflect the concentration at which the Fermi energy reaches the continuum of delocalized states.

Currently the theoretical description of the metallic phase which exists above this critical value of δ is far from complete, and even the nature of the quasiparticles which carry current is controversial. There are, however, two main points of view. In one, metallic conduction results from a band of $N(1-\delta)$ electrons (N is the density of sites), whose excitations at low frequency and temperature can be described in terms of Fermi-liquid theory (FLT). The quasiparticle mass is greatly enhanced by the local Coulomb interaction, and diverges as $1/\delta$ as the insulating phase is approached.[35] Another viewpoint is that FLT does not apply to the metallic phase, and that the metallic conduction is mediated by $N\delta$ positive carriers which are spin singlets.[7] The quantum statistics of these quasiparticles is not agreed upon at present. These two points of view lead to qualitatively similar behavior for $\sigma(\omega,T)$ at low ω, so our analysis of σ will not enable us to distinguish between them. Given the necessity of having a definite language in which to describe our results, we will generally refer to the picture of $N\delta$ positive carriers, or "holes," although our analysis is independent of this model and can be compared as readily with calculations based on FLT.

In the metallic state, σ is expected to consist of two basic components: a free-carrier contribution from the $N\delta$ holes, centered at $\omega=0$ and charge-transfer transitions at much higher frequency which remain from the insulating phase. The free-carrier component is itself expected to separate into "coherent" and "incoherent" components due to the interaction of carriers with phonons, and spin and charge excitations of the electrons. The effect of these interactions is expected to be analogous to the usual carrier-phonon interaction. The coherent component, which remains centered at $\omega=0$, contains the spectral weight associated with the translational motion of the carrier moving together with a cloud of virtual excitations. The remainder of the free-carrier spectral weight, the "incoherent" component, corresponds to optical transitions in which the carrier is excited out of its local distortion, leaving behind real excitations. This component occurs at frequencies characteristic of these excitations. The ratio of the total free-carrier spectral weight N_{free} (proportional to $\delta m/m_0$) to the coherent component, defines the low-frequency mass enhancement, m^*/m_0. In theoretical models in which the regime of small δ is emphasized, the dominant interaction of carriers is with the short-range fluctuating AF order which is the remnant of the infinite-range order of the insulating phase.[35–37] The mass enhancement which results from this interaction is expected to depend on the ratio J/t, where J is the AF exchange coupling energy.[38]

2. Conductivity in the metallic phase: Free-carrier and interband contributions

In this section we analyze the development of σ beyond the insulator-to-metal transition in $YBa_2Cu_3O_{6+x}$. The essential first step in this analysis is to identify the contribution to σ from the free carriers, in which we are primarily interested, as opposed to contributions from electrons in bands which do not intersect the Fermi energy. The behavior of σ as a function of O content, which is illustrated in Fig. 5, plays a crucial role in this identification. The spectra shown in Fig. 5 appear to contain at least two components: a narrow peak centered at $\omega=0$ and a broad component that extends throughout the frequency range within the gap in the insulating phase. These components of σ increase with increasing x; however, the rate of growth is not uniform. Spectral weight increases most rapidly for $\omega < 5000$ cm^{-1}, and is nearly independent of O content for $\omega > 10\,000$ cm^{-1}.

We associate the narrow component centered at $\omega=0$ with at least part of the contribution of free carriers to σ. This assignment is suggested by the observation that the area under this peak grows rapidly with increasing O content, as expected for the generation of carriers by withdrawal of electrons from the CuO_2 layers. Additional evidence comes from the temperature dependence of σ, which is shown for all of the metallic samples in Figs. 8(a)–8(d). These spectra show that the peak at $\omega=0$ narrows and increases in height with decreasing temperature, and that the extrapolated values of σ at $\omega=0$ are consistent with the T^{-1} dependence of $\sigma(0)$ obtained from dc transport experiments.[39]

While it seems clear that the T-dependent peak at $\omega=0$ can be attributed to the response of free carriers, this component is not necessarily their only contribution to σ. The discussion in the preceding section indicated that an incoherent contribution from the free carriers, shifted away from $\omega=0$ is expected due to interactions, such as carrier spin. In other models, low-frequency contributions from itinerant carriers result from transitions from the Fermi energy to low-lying bands.[40] The signature of both processes is that their spectral weight should scale with the carrier concentration $N\delta$. In contrast, contributions to σ which involve bands removed from the Fermi energy will depend only weakly on δ. Our plan for separating σ into free-carrier and interband components

is the following. We first determine the spectral weight in the $\omega=0$ peak, which is proportional to the free-carrier concentration, for each of the metallic samples. We then analyze the broad component at higher frequencies to see what portion scales with δ. The remaining conductivity at higher frequency, which is nearly independent of δ, we associate with other transitions.

We begin this analysis with a description of the spectral weight in the peak at $\omega=0$. In order to estimate this spectral weight, we have fit the spectra of the metallic samples, at low ω, to a Lorentzian of the form

$$\sigma(\omega)=\frac{\omega_p^{*2}\Gamma^*/4\pi}{\omega^2+\Gamma^{*2}} .$$

The plasma frequency, ω_p^*, determined from this fit, can be converted to an equivalent spectral weight [per Cu(2) site] through the relation

$$N_{\rm eff}^*\equiv\frac{\omega_p^{*2}}{4\pi n_{\rm Cu(2)}e^2/m} ,$$

where $n_{\rm Cu(2)}$ is the density of Cu(2) sites. $N_{\rm eff}^*$ and ω_p^* are given in Table I for each of the metallic samples.

Before discussing the broad component of σ at higher energy, we compare $N_{\rm eff}^*$ with expectations based on the theoretical ideas presented in Sec. IV B 1. Recall that the total free-carrier spectral weight was predicted to be $\delta m/m_0$. Direct comparison with $N_{\rm eff}^*$ is complicated by the fact that neither δ nor m_0 are known very accurately, although useful bounds can be estimated. For samples with $T_c\simeq 90$ K ($x\simeq 1$), estimates of δ based on chemical valence arguments range from 0.33 to 0.5, depending on how the holes are distributed between plane and chain sites. The latter value is supported by a recent measurement of the Hall effect in Ni-doped samples, which yielded a T-independent Hall resistance.[41] The value of m_0 is also difficult to ascertain with great precision. In principle, the m_0 appropriate for any δ can be calculated if the value of the hopping-matrix element t is known. However, t depends on the degree to which the suppression of Cu-O hopping by U_{dd} is taken into account. A reasonable lower limit of $m_0\simeq 0.6m$ can be found by estimating t from the dispersion in the band structure,[31,32] and an upper limit of $m_0\simeq m$ can be estimated by considering only direct O-O transfer.[42]

The calculated lower bound for $N_{\rm eff}^*$, for samples with $T_c=90$ K, is 0.33 (assuming the smaller value for δ and the larger for m_0), which is significantly larger than the experimental value of 0.14 for $N_{\rm eff}^*$ (see Table I). This requires that the $\omega=0$ peak contains only part of the free-carrier spectral weight, and that the remainder is at higher energy.

TABLE I. Summary of the spectral weight in the coherent, or Drude-like, component of the optical conductivity, and comparison with the spectral weight in the superfluid.

Sample	T_c (K)	$N_{\rm eff}^*$	ω_p^* (eV)	$\omega_{\rm sf}$ (ev)
$YBa_2Cu_3O_{6+x}$	90	0.14	1.50	1.4
$YBa_2Cu_3O_{6+x}$	80	0.11	1.35	
$YBa_2Cu_3O_{6+x}$	50	0.065	1.00	0.9
$YBa_2Cu_{3-y}Al_yO_{6+x}$	30	0.03	0.70	

To identify the remainder of the free-carrier spectral weight, we examine quantitatively the growth of σ at higher frequencies with increasing O content. Specifically, we look for the component which increases in proportion to $N_{\rm eff}^*$. For each sample we write the total spectral weight (up to 2 eV) N_T as the sum of free-carrier and interband components, $N_{\rm free}+N_{\rm inter}$. If the free-carrier contribution is proportional to $N_{\rm eff}^*$ then $N_{\rm free}=(1+\lambda)N_{\rm eff}^*$, where $1+\lambda$ is the enhancement factor and

$$N_T=(1+\lambda)N_{\rm eff}^*+N_{\rm inter} .$$

If λ is independent of δ in the range covered by our samples, then a plot of N_T versus $N_{\rm eff}^*$ will fall on a straight line with slope $1+\lambda$ and intercept $N_{\rm inter}$. We have carried out this procedure and find a reasonably straight line with values of $\lambda=1.3$ and $N_{\rm inter}=0.3$ carriers per cell.

The preceding arguments suggest a division of the total spectral weight in σ below 2 eV into free-carrier and interband components, with the free-carrier contribution equal to $(1+\lambda)N_{\rm eff}^*$. The spectra in Fig. 5 suggest that the free-carrier spectral weight lies below ≈ 1 eV, corresponding to the frequency range in which σ grows most rapidly with increasing O content. The total free-carrier spectral weight for he $T_c=90$ K sample is $(1+\lambda)N_{\rm eff}^*$, or 0.32, consistent with the theoretical expectation for $\delta m/m_0$ discussed previously. Reflectivity measurements in both $YBa_2Cu_3O_{6+x}$ and $La_{2-x}Sr_xCuO_4$ also support the idea that interband transitions are important at $\omega\sim 1$ eV. Measurements on small untwinned domains of $YBa_2Cu_3O_{6+x}$ crystals show that the absorption above ~ 1 eV is stronger for polarization along the b axis, suggesting that an interband transition involving the O-Cu-O chains accounts for much of the spectral weight in this range.[43] In $La_{2-x}Sr_xCuO_4$ thin films, Suzuki[44] has measured both optical transmission and reflection in the frequency range from 0.5 to 3.0 eV. He finds that, in metallic samples, there is a feature with an onset at ≈ 1 eV, which implies that above this energy the absorption is not primarily due to the free carriers.

With this estimate for the free-carrier spectral weight, we can estimate the low-frequency mass enhancement of the holes. Recall from Sec. IV B 1 that the mass enhancement at $T=0$ is defined by the ratio of the total free-carrier spectral weight to the coherent component. In order to completely separate the spectral weight in the coherent peak from the incoherent part, it is necessary that the temperature be low compared with the energy of the excitations which interact with the free carriers. The observation that σ is T-dependent at 100 K indicates that there are excitations at an energy $\sim k_BT$ which contribute to the scattering, and therefore the mass renormalization, of free carriers. In the next section we will see that the coupling strength to these low-frequency excitations must be weak in order to account for $\sigma(\omega,T)$ near $\omega=0$. Because this interaction is weak, even though the parts of the spectrum are not separated, $N_{\rm eff}^*$ is an excellent ap-

proximation to the coherent spectral weight, and the ratio of the total weight to $N^*_{\rm eff}$, $1+\lambda \simeq 2.3$, is a reasonable estimate of the mass enhancement. It is interesting that the interaction of the holes with other excitations, as expressed through this mass enhancement, is not exceptionally strong. Similar mass enhancements have been observed in Pb, Hg, and Nb_3Sn, for example, and attributed to electron-phonon coupling.[45] It should be remembered that describing the carriers as "holes" absorbs into the carrier density ($N\delta$) the strong renormalization due to the short-range Coulomb repulsion, which leads to insulating behavior for $\delta=0$.

C. Fitting $\sigma(\omega,T)$ with an $\alpha^2F(\omega)$

In the previous section we presented evidence for an enhancement of the free-carrier mass at low frequency. Mass enhancement is generally considered to result from the interaction of carriers with other (usually low-frequency) excitations of the solid. The goal of this section is to see whether quantitative information on the spectrum and coupling strength of these low-lying excitations can be determined from fitting the measured $\sigma(\omega,T)$.

As discussed in Sec. IV B, the qualitative effect of inelastic scattering of carriers is to separate $\sigma(\omega,T)$ at low temperature into coherent and incoherent components. Joyce and Richards[46] first observed (in Pb) the incoherent absorption, predicted by Holstein,[2] which arises from the electron-phonon interaction. Allen[47] showed that $\alpha^2F(\omega)$, the product of the square of the electron-phonon vertex and the phonon density of states, can be determined from $\sigma(\omega,T)$. In addition, he pointed out that the underlying physics is not unique to the electron-phonon interaction, and that in metals in which the carrier-spin interaction dominates, $\sigma(\omega,T)$ may reflect the $\alpha^2F(\omega)$ appropriate for magnons. In the following we briefly outline the relation between $\sigma(\omega,T)$ and $\alpha^2F(\omega)$, and then compare the frequency and temperature dependence expected from the inelastic scattering with our experimental results.

It is useful to discuss the $\sigma(\omega,T)$ predicted by the Holstein model in two limits: high and low temperature. The crossover between these limits occurs when T is comparable to an average boson frequency Ω_0 where

$$\Omega_0 \equiv \frac{2}{\lambda}\int_0^\infty \alpha^2F(\omega)d\omega$$

and

$$\lambda \equiv 2\int_0^\infty \frac{\alpha^2F(\omega)}{\omega}d\omega \ .$$

For $T>\Omega_0$, $\sigma(\omega)$ is Lorentzian, and the scattering rate of carriers Γ has the ω-independent value $2\pi\lambda k_BT$. At low temperatures, σ deviates from this simple form, and both Γ, and the carrier mass, become frequency dependent. As ω tends to zero, the mass enhancement m^*/m_0 approaches $1+\lambda$.

In order to compare this model with our experimental results, we have calculated $\sigma(\omega,T)$ for a variety of reasonable choices for $\alpha^2F(\omega)$. We found that it was not possible to obtain a reasonable fit. With hindsight, the reason is that the calculated $\sigma(\omega,T)$ is highly constrained within the Holstein picture in the following way. A particular $\sigma(\omega,0)$, or $\sigma(0,T)$, tightly constrains the possible functions $\alpha^2F(\omega)$, which, in turn, uniquely determine $\sigma(\omega,T)$. In particular, we have found that fitting the linear $\sigma^{-1}(0,T)$ makes it impossible for us to fit $\sigma(\omega,T)$ over the range of ω in Fig. 8.

The argument can be phrased most simply in terms of the fermion-boson coupling strength λ which can be determined from the low frequency-behavior of $\sigma(\omega,T)$. The observation that $\rho_{\rm dc}$ versus T is linear suggests that the high-T_c materials (in the normal state) are in the high-temperature limit of the scattering process, in which $T \gtrsim \Omega_0$ and $\Gamma = 2\pi\lambda k_BT$. From the fitting procedure described in Sec. IV B, we found that $\Gamma^* \lesssim 2k_BT$, where Γ^* is the width at half maximum of a Lorentzian centered at $\omega=0$, which implies that $\lambda \simeq 1/\pi$. In contrast, $\lambda \simeq 1.3$ was inferred from the ratio of the total free-carrier spectral weight to the coherent component. This discrepancy indicates that the smaller values of λ determined from the low-frequency properties will fail to describe the part of $\sigma(\omega,T)$ at higher frequencies that we identify with free carriers. (As noted above, we exclude an interband part at a still higher frequency from the start.)

The difficulty in fitting $\sigma(\omega,T)$ over a broad frequency range is illustrated in Fig. 10, in which the experimentally determined $\sigma(\omega)$ of the sample with $T_c=90$ K is plotted as solid circles. The theoretical curves were obtained by first calculating the self-energy (using the Midgal approximations[48]) for electrons interacting with a spectrum of dispersionless oscillators, and then using the Kubo for-

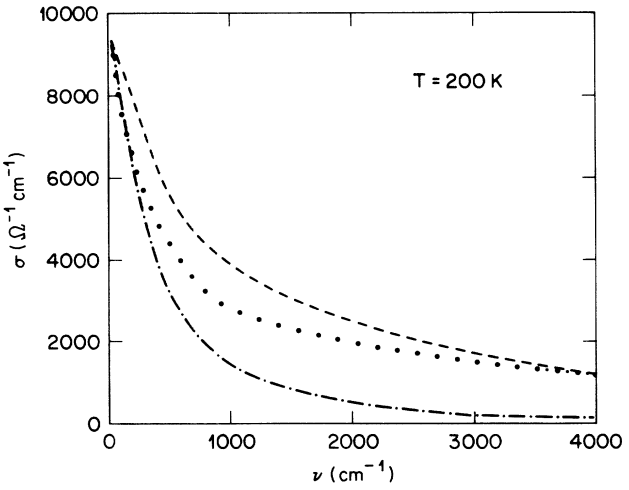

FIG. 10. Conductivity as a function of frequency for the crystal with $T_c=90$ K at $T=200$ K (solid circles). These data are compared to two fits with parameters defined in the text: dash-dotted curve: $\omega_p^*=1.4$ eV, $\lambda=0.4$; dashed curve: $\omega_p^*=2.15$ eV, $\lambda=2.0$. Parameters can be chosen (within the weak scattering model) that describe the data at low frequency and at dc (dash-dotted curve), and indicate an added absorption above $\nu \sim 500$ cm^{-1}. Alternatively, stronger scattering could describe the large σ near 4000 cm^{-1}, but cannot fit the results over the frequency region shown.

mula[49] to compute $\sigma(\omega,T)$. We assumed an $\alpha^2F(\omega)$ with $\Omega_0=330$ cm^{-1} and width $\simeq 500$ cm^{-1} which was found to yield the closest approximation to these data of the set of functions that we tried. We varied the coupling strength λ and the plasma frequency which corresponds to the coherent spectral weight ω_p^* [which scales $\sigma(\omega)$ without changing its shape]. The dash-dotted and dashed curves use $\omega_p^*=1.4$ eV, $\lambda=0.4$, and $\omega_p^*=2.15$ eV, $\lambda=2.0$, respectively. As anticipated, the relatively small λ, which describes σ for small ω, is not consistent with the large spectral weight at higher frequency. Increasing λ and ω_p^* to account for the mid-infrared spectral weight (dashed curve) results in a low-frequency scattering rate and spectral weight which is larger than found experimentally. It seems, therefore, that at least two processes are required to understand the form of $\sigma(\omega,T)$ over this range of frequency (below $\sim\frac{1}{2}$ eV). The first, required by $\Gamma^*(T)$ (the Drude-like half-width), is a weak interaction with modes at low frequency. The second interaction must be stronger to account for the mass enhancement and higher-frequency absorption. In the following discussion we consider coupling to phonons as a candidate for the low-frequency interaction and then briefly comment on the higher-energy process.

Given the relatively small value of λ inferred from $\Gamma^*(T)$, electron-phonon coupling should be considered (as well as more exotic mechanisms) to explain $\sigma(\omega,T)$ for small ω. The major argument against phonons is that ρ_{dc} is linear to lower temperature than is consistent with the phonon density of states (PDOS). To see if the argument is valid, we have calculated Γ_{ph}, the scattering rate due to phonons, using an $\alpha^2F(\omega)$ which roughly simulates the PDOS. Figure 11 illustrates the results of these calculations. The lower of the two dashed lines shows Γ_{ph} for $\lambda=0.4$ and an $\alpha^2F(\omega)$ which is constant from 10 to 80 meV, the range of phonon energies measured by neutron scattering.[50] For comparison, Γ_{ph} resulting from a sharply peaked DOS, with the same λ and Ω_0, is plotted with dots. The limiting behavior at high temperature, $2\pi\lambda k_BT$, is shown by the solid line. Finally, the higher of the dashed lines illustrates the effect of adding a contribution Γ_{el}, due to elastic impurity or defect scattering, to the Γ_{ph} resulting from the broad PDOS.

The calculations presented in Fig. 11 suggest that an explanation for Γ^* based on the combined effect of phonon and defect scattering is consistent with the experimental data on crystals with high T_c's. Similar analysis has been presented by Kim *et al.*[51] Measurements in materials with lower T_c's, for example, the $La_{2-x}Sr_xCuO_4$ compounds, provide a more stringent test of the phonon-scattering hypothesis. Transport data on highly oriented thin films show large residual resistivities and a flattening of ρ versus T for $T\lesssim 100$ K,[44] and are consistent with the calculations shown in Fig. 11 for reasonable values of Γ_{el}. However, recent evidence that ρ_{dc} versus T is linear for $20<T<300$ K in a Bi-Ca-Sr-Cu-O compound is difficult to explain with phonon scattering.[52] Regardless of whether the important low-frequency excitations are phonons, the model calculation illustrated in Fig. 11 shows that weak coupling to a broad spectrum of modes is consistent with $\Gamma^*(T)$.

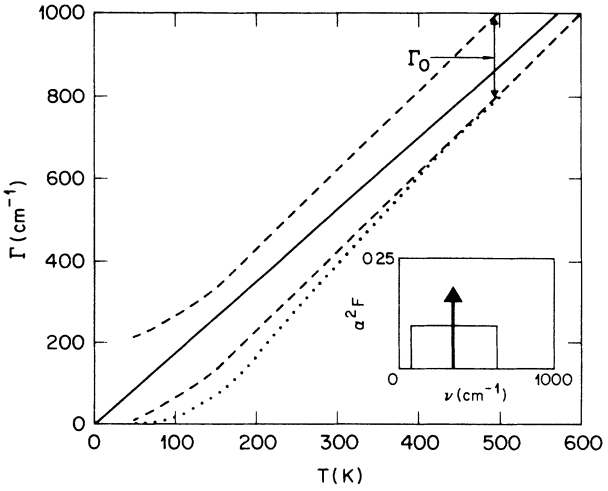

FIG. 11. Scattering rate Γ as a function of temperature calculated using the inelastic scattering model described in the text, in which $\alpha^2F(\omega)=\lambda/2\ln(\omega_h/\omega_l)$ for $\omega_l<\omega<\omega_h$, $\alpha^2F(\omega)=0$ otherwise. The three curves correspond to the following sets of parameters: (curve: ω_l, ω_h, Γ_0) = (lower dashed, 10 meV, 80 meV, 0), (upper dashed, 10, 80, 200 cm^{-1}), (dotted, 44, 46, 0). The $\alpha^2F(\omega)$ functions are illustrated in the inset to the figure. In each of the curves $\lambda=0.4$. The solid, straight line shows the high-temperature limit of the scattering rate $2\pi\lambda k_BT$. The figure illustrates that a simple $\alpha^2F(\omega)$ can be chosen which produces a linear dependence of Γ (and σ_{dc}^{-1}) on T.

Having seen that ρ_{dc} may be fit by inelastic scattering from low-frequency excitations, we turn now to a comparison of $\sigma(\omega,T)$ arising from the same model with the experimental data. Figure 12 shows this comparison for the sample with $T_c=50$ K. The measured $\sigma(\omega)$, for the three temperatures indicated in the figure, are plotted as solid circles. The solid line shows normal state $\sigma(\omega)$ calculated using the broad $\alpha^2F(\omega)$ shown in Fig. 11 and $\omega_p^*=1.0$ eV. The dashed line shows the difference between theory and experiment. As the difference curve highlights, there is a component of σ, beginning at ≈ 50 meV, which is not accounted for by the same mechanism which describes σ at low frequency. This is basically the same extra absorption that is illustrated in Fig. 10. In the superconducting state (bottom panel of Fig. 12), a feature appears directly in σ at ≈ 50 meV (without subtraction of a theoretical curve). The appearance of this feature in σ is a major theme of the next section, which discusses the development of the optical properties in the superconducting phase.

D. Superconducting phase

In this section we discuss the changes in reflectivity which occur as the metallic crystals are cooled below T_c, and the question of determining the magnitude of the superconducting gap 2Δ from the optical data. There are two features in $R(\omega)$ which appear as the sample temperature is lowered at ~ 150–200 cm^{-1} (18–24 meV) and at

~ 400 cm^{-1} (50 meV). The higher-energy feature is observed in samples of varying quality, while the lower-energy feature is not seen in samples which have a lower overall R than those reported in this paper. A study of the systematics of these sample to sample variations has been reported previously.[10] In Sec. IV D 1 we focus on the behavior of these features in high-R crystals with different free-carrier concentration and T_c, and compare this behavior with expectations for an energy gap as described by the BCS theory of superconductivity.[53] In Sec. IV D 2 we briefly review the theoretical prediction for $\sigma(\omega,T)$ in a BCS superconductor near the gap frequency Δ, emphasizing the importance of the relative magnitudes of Δ and the elastic scattering rate Γ_{el}. We then compare qualitatively these predictions with the experimental spectra. Finally in Sec. IV D 3 we compare the optical reflectivity spectra with data obtained by other spectroscopic techniques which probe the same energy range.

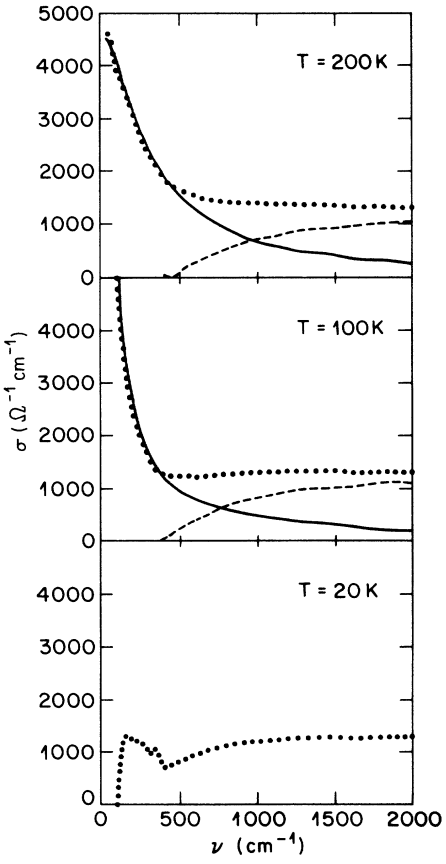

FIG. 12. Conductivity as a function of frequency for a crystal with $T_c = 50$ K for three temperatures as indicated (dotted line), compared to a calculation of the weak scattering model (solid lines) presented in Figs. 10 and 11. Data are smoothed as described above. The calculation uses the broad scattering distribution of the inset to Fig. 11, a plasma frequency of 1.0 eV, and a coupling of 0.4. The dashed curves are the difference between the fit and the data. The comparison illustrates a nearly T-independent component of the spectrum (present most clearly below T_c) that begins near 400 cm^{-1} (50 meV) and is not adequately described by the inelastic scattering model.

1. *Trends with T_c and carrier concentration*

Consider first the reflectivity at low ω and T of the sample with a T_c of 90 K which is shown in the bottom panel of Fig. 7. $R(\omega)$ which is featureless and nearly linear at $T = 100$ K, develops structure as T is lowered further. In the 20-K spectrum, R is relatively constant at low ω and its magnitude is consistent with unity, given our experimental uncertainly. Near 400 cm^{-1} there is a "knee" in $R(\omega)$. This feature was observed initially in samples with lower R than those reported in this work.[54,55] Measurements of relative changes in R versus T showed that the feature appeared near T_c in crystals with $T_c \simeq 90$ K, which led to an identification as the superconducting energy gap.[54] Subsequently, measurements of the absolute magnitude of $R(\omega)$ versus T have been reported by several groups in crystals,[10,56,57] and in thin films,[58,59] with $T_c \simeq 90$ K and significantly higher overall R than those studied initially. These results are in good agreement with each other, and are very similar to the spectra shown in the bottom panel of Fig. 7, which suggests that the intrinsic behavior of $YBa_2Cu_3O_7$ is emerging.

Before considering the $\sigma(\omega)$ which corresponds to $R(\omega)$ in the superconducting state, we wish to describe in more detail the extent of the experimental uncertainly. In Fig. 13 the low-T spectrum of the sample with $T_c = 90$ K is plotted so as to emphasize the size of the experimental uncertainly in R. The shaded region shows the uncertainty due to detector noise, which grows rapidly at low frequency because of the decrease in source intensity. The two horizontal lines depict the 1% absolute uncertainty in R which is due to various sources including the alignment of the reference mirror. Assuming the largest reasonable values, R reaches unity (as ω approaches zero) at ≈ 380 cm^{-1}. Other R spectra that lie within the shad-

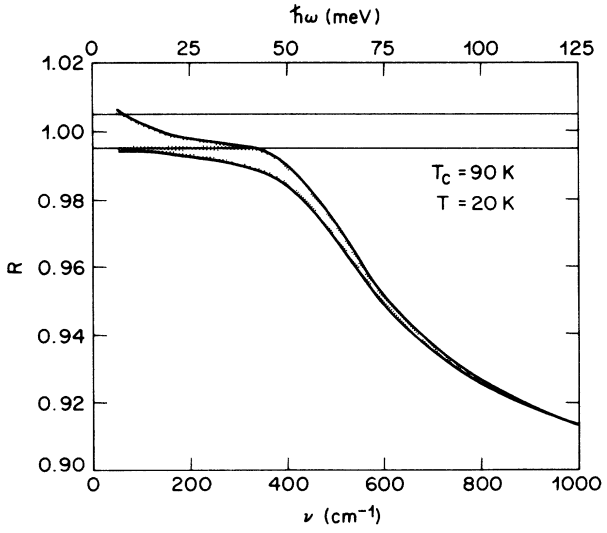

FIG. 13. Reflectivity as a function of frequency for a sample with $T_c = 90$ K at $T = 20$ K. The uncertainty associated with oscillations or noise in the data which have been taken out by smoothing is indicated by the shaded region. The uncertainty associated with the absolute magnitude of R is indicated by the two solid lines located 0.005 above and below $R = 1$.

ed region approach unity smoothly as ω tends to zero. Because R is close to unity at low ω, these relatively small differences map into large differences in the corresponding σ obtained by KK transformation. Several $\sigma(\omega)$ consistent with the uncertainty in $R(\omega)$ are illustrated in Fig. 14. If we assume that $R=1$ below a frequency ω_0, then $\sigma=0$ for $0<\omega<\omega_0$, and $\sigma(0)\sim\delta(0)$. The solid curves in Fig. 14 show $\sigma(\omega)$ which correspond to two choices for ω_0, one near the position of the "knee" in R at ≈ 400 cm^{-1} and the other $\omega_0=150$ cm^{-1}. Notice that the assumption $\omega_0=150$ cm^{-1} produces two features in $\sigma(\omega)$, one corresponding to the knee in R and the other to the onset of absorptivity $A\equiv 1-R$ at ω_0. The dashed and dot-dashed curves in Fig. 14 correspond to R spectra which approach unity smoothly as ω goes to zero. If A is proportional to ω^2, then σ tends to a finite, nonzero value as ω approaches zero.[60] If A decreases faster than ω^2, then σ may approach zero as $\omega\rightarrow 0$.

For the sample with $T_c=90$ K, all of the spectra in Fig. 14 are consistent with the data. The edge in σ near 400 cm^{-1}, which is common to all four spectra, is the only feature which is clearly outside the range of experimental error.

In spite of the uncertainty in R, we must choose a procedure for extrapolating to $\omega=0$ in order to perform the KK transformation. For analysis and presentation of the low-T spectra we have assumed that $R=1$ below some ω_0. The choice is motivated primarily by the low-T spectra of crystals with T_c less than 90 K. Previously we have reported R spectra of samples with T_c's of 50 and 68 K for which $A\approx 4\%$ at 400 cm^{-1}. For these samples R is constant (to within 1%) below 110 and 150 cm^{-1}, respectively, and its value is consistent with unity. Similar behavior is observed in the two additional samples with T_c less than 90 K described in the present paper. The R at $T=10$ K for these crystals is shown as a function of ω in Fig. 15, without the smoothing used in previous figures. In all data presented here identifiable oscillations are removed before plotting in a procedure that also removes some indications of phonon absorption. We have accepted this loss of information since we wish to concentrate here on the processes with large spectral weight that change with carrier concentration. These spectra are similar to those reported previously in that R is relatively flat and consistent with unity at low ω.

The σ spectra which result from this assumption have a shape illustrated in Fig. 14; $\sigma=0$ for $\omega<\omega_0$ and has a peak above this frequency. As we have discussed above, it is impossible to rule out a nonzero A on the level of 1%. The σ spectra in the range of frequency where $A\lesssim 1\%$ should be considered in light of Figs. 13 and 14, and our previous discussion.[22]

As a qualitative indication of the large uncertainty in σ, we have used lighter lines for the low-ω part of the data for $T<T_c$ in Figs. 8 and 16, and have plotted error bars in Fig. 17. The absolute uncertainty can be analyzed by considering the data for R shown in Figs. 7 and 15. The ω where σ goes to 0 corresponds to the point where

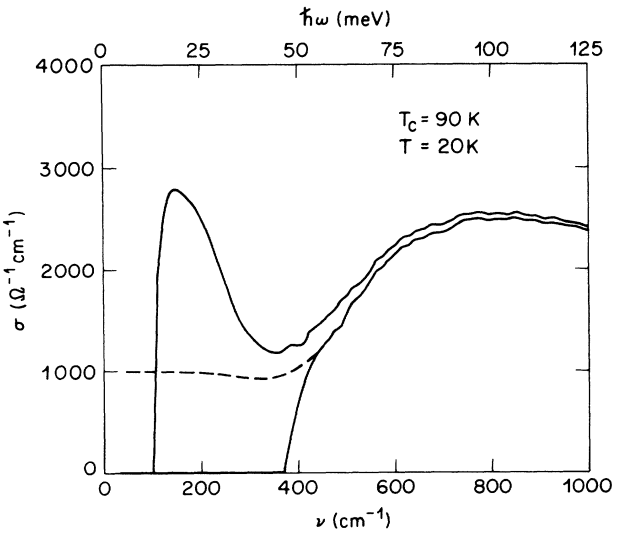

FIG. 14. Conductivity as a function of frequency calculated from the data of Fig. 13. To illustrate the substantial uncertainty in values of σ derived from R where R is near 1, we have shown three behaviors that are possible for this data set when we take into account the uncertainties illustrated in Fig. 13.

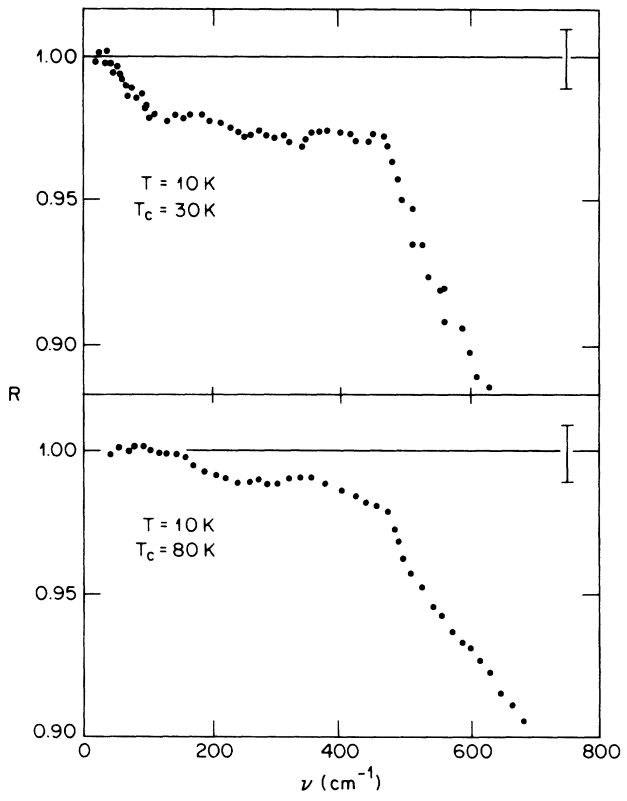

FIG. 15. Reflectivity as a function of frequency for two samples with T_c values as indicated. These data are unsmoothed compared to the results shown in Fig. 7, but identifiable oscillations have been removed. Uncertainties are similar to those indicated in Fig. 13, with the absolute error shown by the bars in the upper right. Similar plots of all of our other samples have been published previously. We argue that it is preferable to consider these plots of R rather than our plots of σ when evaluating the reliability of the low-energy absorption features.

$R=1$ within our best estimate. The uncertainty in σ is extremely large near this point and remains so until the ω above which $A>1\%$ ($R<0.99$). In our data, at this ω, the relative uncertainty in R is smaller than this absolute uncertainty. We have suppressed the relative error by smoothing, but even so, this noise eventually becomes dominant (see, e.g., Fig. 15). At this point, we stop showing data. The $A>1\%$ criterion provides an estimate of the region that should be lightly drawn in Figs. 8 and 16, and of the upper edge of the error bars in Fig. 17. (The lower extent of each error bar is drawn symmetrically, but we cannot rule out $\omega=0$). The samples with reduced T_c provide better information on low-frequency features because A is larger. This larger A results from increased scattering (as a result of O disorder) and lower carrier concentration. The $T_c=90$ K sample shown in Figs. 13 and 14 is the case with the largest uncertainty. We reemphasize[22] that in order to assess the validity of conclusions drawn from data at low ω and low A, it is best to consider the curves for R rather than σ, since the errors in R remain finite (absolute error is a constant 1%), while those for σ diverge. In general, some questions regarding the behavior of $\sigma(\omega)$ at very low ω can be clarified only with improved accuracy. Measurements of transmission through films whose thickness is comparable to λ_L and direct measurements of A by bolometric techniques are, in principle, capable of providing this information.

The σ determined from the reflectivity spectra of Fig. 7 are shown in Fig. 8. The strong T dependence of the features in σ for $T\sim T_c$ suggests a connection with superconductivity. We discuss first the feature at ≈ 400 cm^{-1}, and show that although it may be a gap associated with the superconductivity, its behavior in crystals with reduced T_c argues against an interpretation in terms of a conventional BCS gap.

The R spectra of the reduced T_c samples are shown in panels (a)–(c) of Fig. 8. The knee in R near 400 cm^{-1} is apparent in the spectra of each of the crystals, and its energy appears to be independent of T_c. Although, in the sample for which $T_c=90$ K, the feature appears only at $T_c=90$ K, in the other metallic samples the knee is visible in the normal state. A clear trend is that the feature is increasingly prominent, and observable at higher temperatures, as the free-carrier concentration, and T_c, become smaller. For the sample with the lowest free-carrier concentration and a T_c of 30 K, the structure in R is observable for $T\simeq 270$ K.

The main points of the preceding paragraph are emphasized in Figs. 8(c) and 16. Figure 16 compares $\sigma(\omega)$ in the normal state (at $T=100$ K) with the low temperature $\sigma(\omega)$, for each of the crystals. As before, we assumed $R=1$ at the lowest frequencies in performing the

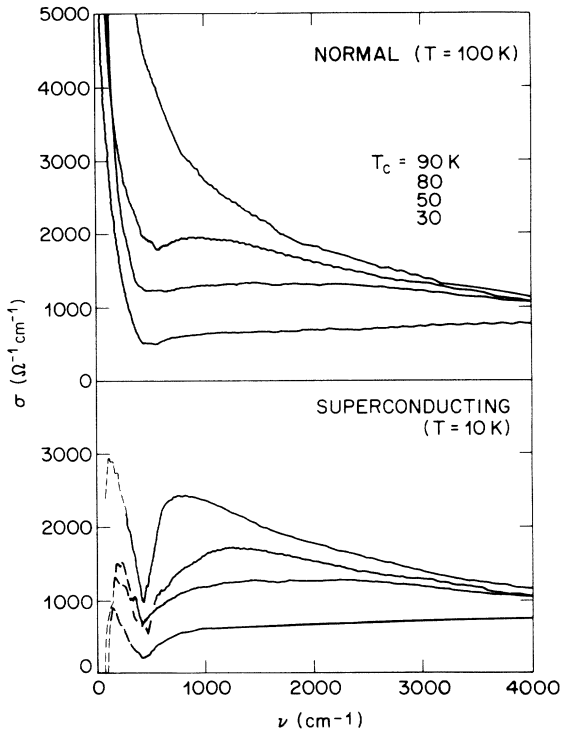

FIG. 16. Comparative overview of the conductivity as a function of frequency for several crystals with T_c values as labeled. The upper part of the figure shows the normal state ($T=100$ K) and the lower part, the superconducting state ($T\sim 10$ K). The dashed lines at low frequency emphasize the uncertainties discussed above.

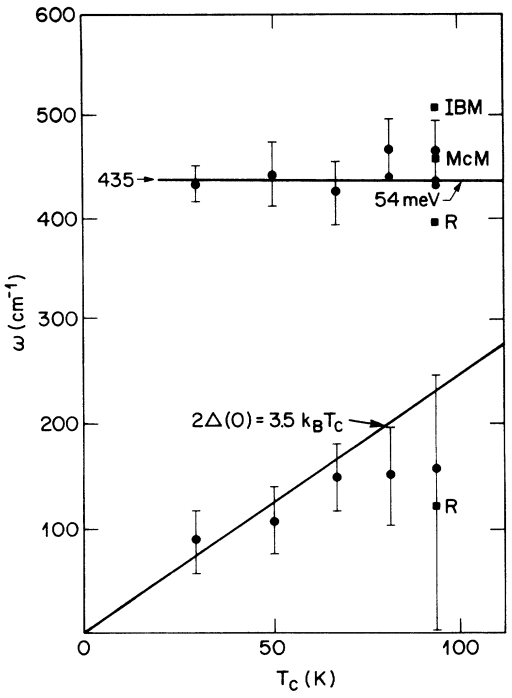

FIG. 17. A summary of the two features in $R(\omega)$ as a function of T_c. The results from Figs. 7 and 8 are shown as solid circles and two additional points are plotted from similar crystals with $T_c=80$ and 70 K. Results from other groups are plotted as solid squares labeled IBM (Ref. 56), McM (Ref. 55), and R (Ref. 57). The line through the upper data indicates the T_c independence of the "knee" in $R(\omega)$, the lower line is the prediction of weak-coupling BCS theory for the superconducting energy gap (not a fit).

KK transformations. The spectra in the superconducting state (lower panel) clearly show that the threshold at $\sim 400\ \mathrm{cm}^{-1}$ is independent of T_c. The normal-state spectra (upper panel) of the reduced T_c crystals indicate that the same feature is present in the normal state, although it appears as a shallow minimum in $\sigma(\omega)$ rather than a pronounced threshold. The temperature dependence of the minimum can be seen more clearly in Fig. 8(c), in which $\sigma(\omega)$ at several temperatures for the sample with $T_c = 80$ K is plotted on an expanded vertical scale. The minimum in $\sigma(\omega)$ is visible in this sample at T as high as 150 K.

The lack of an energy shift (for T above and below T_c) of the absorption threshold at 400 cm^{-1}, and its presence at $T > 90$ K, clearly argue against a simple interpretation in terms of a BCS gap. The strength of the first of these arguments depends on the homogeneity of the O concentration and the degree of ordering. Because the extent of inhomogeneity is not known for our samples, we consider a "worst-case scenario," in which samples with intermediate T_c's consist of "grains" of a homogeneous superconductor separated by normal material. In this scenario, we expect the gap to be constant, independent of the morphological variations which determine the bulk T_c, as has been observed in tunneling measurements on granular superconductors.[61,62] The absence of a shift of the 400-cm^{-1} feature is consistent with the BCS model if there is only one homogeneous superconducting phase in the $YBa_2Cu_3O_{6+x}$ compounds with $T_c = 90$ K. If, however, there are two homogeneous superconducting phases in $YBa_2Cu_3O_{6+x}$ with T_c's of ~ 60 and ~ 90 K, the samples with intermediate values of T_c should have two gap values. This is in contrast to the data, in that the 400-cm^{-1} feature is stronger rather than weaker in the lower-T_c samples and does not separate into two spectral features. Furthermore, evidence for a higher-T_c phase in our reduced T_c crystals is absent in magnetization, dc conductivity, and microwave conductivity, as discussed above.

The second point, that the 400-cm^{-1} feature exists in the normal state well above 90 K, clearly cannot be explained by O inhomogeneity. It is also inconsistent with fluctuations of the BCS order parameter above T_c. In the BCS theory these "Gaussian" fluctuations create small, transient, domains in which the gap is smaller than its magnitude at $T = 0$. In contrast, the spectral feature that we observe occurs at essentially the same energy above and below T_c.

In the frequency range from 150 to 200 cm^{-1} there is another onset in A which has a different dependence on T_c, and T, than the 400-cm^{-1} feature. The energy of this A onset and that of the higher-energy feature are plotted against T_c in Fig. 17, for each of the samples reported in this study. The relatively large error bars indicate the difficulty of measuring A on the 1% level in the far-infrared, particularly for small samples. The lower solid line is the prediction of the BCS theory in the weak-coupling limit $2\Delta = 3.5kT_c$. As is apparent from Fig. 17, the lower-energy threshold varies with T_c for the reduced T_c samples, in a manner which is consistent with the BCS prediction. In addition, this threshold is not present in the normal state of these crystals. These observations suggest that this A onset may correspond to a BCS energy gap. There are, however, several difficulties with this interpretation. The magnitude of A is close to our detection limit, and the feature was only observed in samples with the highest overall reflectivity. Furthermore, as is clear from Fig. 17, the energy of the A onset does not increase as expected in the crystals for which T_c is ~ 90 K. A similar observation was reported recently by Schützmann *et al.*,[58] who achieved a higher signal-to-noise ratio than ours by studying a large area thin film of $YBa_2Cu_3O_{6+x}$ with a T_c of 92 K. They found an onset of A at $\sim 130\ \mathrm{cm}^{-1}$, which corresponds to $2\Delta/k_BT_c = 1.9$.

2. *Comparison with $\sigma(\omega, T)$ for a BCS superconductor*

In this section we present a qualitative description of $\sigma(\omega, T)$ in a BCS superconductor and compare this picture with our experimental results. According to the BCS theory, the dipole moment is zero for a transition from the ground state to the optically accessible ($q = 0$) particle-hole excitations of the superconductor.[63] As a result, elastic scattering, which allows dipole-active excitations with $q \neq 0$, plays a critical role in determining $\sigma(\omega)$ in the superconducting state. The familiar picture of a prominent threshold for optical absorption at 2Δ (as in the Mattis-Bardeen[64] theory) arises when impurity, or surface, scattering is sufficiently strong that the elastic scattering rate Γ_{el} is much greater than the gap parameter Δ. If we imagine turning off the superconductivity at $T = 0$, then in this "dirty" limit, $\Gamma_{el} \gg \Delta$, the normal-state conductivity σ_N is nearly constant on the frequency scale of Δ. Restoring the superconductivity opens a gap at the Fermi energy, and $\sigma_S(\omega)$, the conductivity in the superconducting state, goes to zero in the range $0 < \omega < 2\Delta$. At $\omega = 2\Delta$, there is a threshold in conductivity, and σ_S approaches σ_N for $\omega > 2\Delta$. The spectral weight, which disappears from $0 < \omega \lesssim 2\Delta$, appears in a δ function at $\omega = 0$, which represents the electrodynamic response of the superfluid condensate.[24] The spectral weight in the condensate is a small fraction, $\sim \Delta/\Gamma_{el}$, of the total free-carrier spectral weight.

Both σ_N and σ_S change dramatically as the superconductor is made cleaner. As the clean limit, in which $\Gamma_{el} \ll \Delta$, is approached, the coherent (Drude-like) component of σ_N becomes narrow on the frequency scale of the gap. As before, when the superconductivity is restored, the spectral weight near and below 2Δ goes into the condensate. For the clean superconductor, this represents almost all of the coherent spectral weight, and only a small fraction of the coherent part, $\sim \Gamma_{el}/\Delta$, is associated with particle-hole excitations which begin at 2Δ.

The analysis of $\sigma(\omega, T)$ presented in Secs. IV B and IV C, suggests that the crystals in this study are clean superconductors, because it implies that almost all of the coherent spectral weight of the free carriers appears in the condensate for $T \ll T_c$. The free-carrier spectral weight was estimated in Secs. IV B and IV C, and sum-

marized in Table I. The condensate spectral weight can be determined in two ways: from the difference between N_{eff} in the normal and superconducting states (see Fig. 9) and from measurements (by muon spin rotation, for example) of the London penetration depth at low temperature $\lambda_L(0)$.[65] [$\lambda_L(0)$ is equal to c/ω_{sf}, where ω_{sf} is an effective plasma frequency corresponding to the superfluid spectral weight.] These two measures of the condensate spectral weight yield consistent values for ω_{sf} and, as Table I shows, there is a close correspondence between ω_{sf} and ω_p^*, the effective plasma frequency which corresponds to the coherent component of the free-carrier spectral weight. This correspondence suggests that, within the uncertainly of our estimates, essentially the entire coherent component of the free-carrier spectral weight appears in the superfluid condensate at $T=0$, a condition which defines a clean superconductor.

For clean superconductors, only a small fraction of the spectral weight σ, $\sim\Gamma_{\text{el}}/\Delta$, should appear in the transitions which create particle-hole pairs at 2Δ. To compare the experimental spectra quantitatively with this prediction we can estimate Γ_{el} for our crystals. Because $\sigma(\omega)$ is T dependent at 100 K, it is clear that Γ_{el} must be significantly smaller than Γ^* (the width at half maximum) at 100 K, which is $\sim 140\ \text{cm}^{-1}$. We can also estimate Γ_{el} by referring to measurements of $\rho_{\text{dc}}(T)$. If we assume that the inelastic scattering rate is proportional to T, then a linear extrapolation of $\rho_{\text{dc}}(T)$ to $T=0$ provides a rough measure of the elastic scattering rate. Assuming the validity of Mathiesson's rule, that the total scattering rate $\Gamma(T)$ is the sum of Γ_{el} and Γ_{in}, then

$$\Gamma_{\text{el}} \simeq \Gamma(T_1)\frac{\rho(0)}{\rho(T_1)} ,$$

where T_1 is a temperature at which inelastic scattering dominates, and $\rho(0)$ is the extrapolated intercept at $T=0$. Transport measurements on samples from the same batches as ours have resistance ratios which are in the range

$$0 < \frac{\rho(300\ \text{K})}{\rho(0)} \lesssim 6 ,$$

(Ref. 66) which implies that $0<\Gamma_{\text{el}}<\sim 65\ \text{cm}^{-1}$, for $\Gamma(300\ \text{K})\simeq 400\ \text{cm}^{-1}$. If the threshold at $\sim 400\ \text{cm}^{-1}$ corresponds to a BCS gap, then $\Delta\sim 200\ \text{cm}^{-1}$ and $0<\Gamma_{\text{el}}/\Delta<0.3$. For these samples only a small fraction of the free-carrier spectral weight should appear in particle-hole excitations which begin at 2Δ. Instead, we found in the previous sections that most of the spectral weight of free carriers is at $\omega>50$ meV. Furthermore, the strength of the transition should vary as $\Gamma_{\text{el}}/\Delta$, i.e., be greater in samples with larger elastic scattering rate. In contrast, we found that the strength of the feature at $\sim 400\ \text{cm}^{-1}$ is relatively insensitive to the sample quality, and in the highest conductivity (reflectivity) samples the threshold is sharpest. These arguments suggest that the absorption threshold at $\sim 400\ \text{cm}^{-1}$ is different than the gap transition of BCS in that it appears to be dipole-allowed at $q=0$.

3. *Comparison with other techniques*

In this section we discuss the implications of recent experiments which probe, in different ways, the excitations of the cuprate superconductors in the same energy range as the optical reflectivity. Comparison of optical data with photoemission (PE), tunneling, nuclear magnetic resonance (NMR), neutron scattering (NS), and Raman spectroscopy (RS), is particularly useful. RS is similar to optical reflectivity, although the coupling to particle-hole excitations arises from different matrix elements than $\sigma(\omega)$. Thresholds at 340 and 510 cm^{-1} are observed for $T<<T_c$, depending on polarization,[67,68] which are close in energy to the higher-energy threshold in $\sigma(\omega)$. The main difference is that instead of a second feature at lower energy, the Raman intensity approaches zero smoothly with decreasing frequency.

PE and tunneling are informative because they probe the one-particle DOS, in contrast with optical experiments which measure the DOS for particle-hole excitations. Recent PE experiments[69,70] performed on the $T_c=83$ K phase of $Bi_2Sr_2CaCu_2O_8$ show a shift of the emission threshold (by ~ 30 meV) and a pileup of intensity at threshold, which are highly suggestive of gap formation. The energy scale of this shift and of the gaplike features observed in tunneling experiments[71] in $YBa_2Cu_3O_7$ and $Bi_2Sr_2CaCu_2O_8$ correspond reasonably well to half the energy of the threshold in $\sigma(\omega)$ at ~ 50 meV. This correspondence suggests that the structure in $\sigma(\omega)$ is due to particle-hole excitations across a gap at E_F. In contrast, a strong-coupling feature in the density of states would not have this simple relationship, but would occur at $\Delta+\Omega_0$ and $2\Delta+\Omega_0$ for one- and two-particle probes, respectively.

The comparison of one- and two-particle spectroscopies strongly suggests the existence of a gap of magnitude 50–60 meV in superconductors with $T_c\approx 90$ K. We have argued in Sec. IV D that the variation of the optical gap with T in a given sample, and the variation with T_c in a series of samples, is inconsistent with BCS theory. It is natural to ask whether other probes find evidence for similar anomalies. As yet, studies of PE in superconductors with varying T_c and carrier concentration have not been reported. There are reports of tunneling experiments on $YBa_2Cu_3O_{6+x}$ (Refs. 72 and 73) and $La_{2-x}Sr_xCuO_4$ (Ref. 74) in which, in contrast to our optical results, the (large) energy of a gaplike feature in the spectra varies linearly with T_c. Reports of NS and NMR experiments show anomalies which are analogous to those we find optically. NMR measurements of T_1^{-1}, the nuclear spin-relaxation rate, probe the intensity of electronic spin fluctuations near $\omega=0$, while NS, in favorable situations, can reveal their full frequency and wave-vector dependence. NMR experiments show that, in $YBa_2Cu_3O_{6+x}$ with $x\simeq 1$ and $T_c\simeq 90$ K, T_1^{-1} is nearly constant in the normal state,[75,76] in contrast with the linear dependence on T expected for a T-independent density of states. In cuprate superconductors with lower carrier concentration and T_c (e.g., $La_{2-x}Sr_xCuO_4$ and $YBa_2Cu_3O_{6.7}$), T_1^{-1} begins to decrease, with decreasing T, in the range 150–200 K.[77,78] Recently reported NS mea-

surements appear to show a related effect.[79] In a crystal of $La_{1-x}Sr_xCuO_4$, the spin-fluctuation intensity (at energies below 9 meV) begins to decrease at $T \simeq 150$ K, while above 12 meV the intensity is T independent. Both NMR and NS results suggest that the spin-excitation spectrum is T dependent in the normal state, perhaps indicative of the development of a gap. The interpretation of these experiments is at an early state, and more work is needed to extract the spin-excitation spectrum from the ω and T dependence of the spin fluctuations.

A synthesis of the optical, magnetic, and tunneling spectroscopies of low-energy excitations in the cuprate superconductors suggests that there is a gap at E_F related to electron pairing. However, the properties of this gap differ from the BCS prediction in important ways, namely the magnitude relative to T_c, the existence at $T > T_c$ and the constancy of its value versus T_c. This departure from the BCS behavior is reminiscent of some layered metals which have a charge-density-wave (CDW) ground state, for example $2H$-$TaSe_2$.[80] In this material, $2\Delta_{CDW} \simeq 30 k_B T_{CDW}$, and furthermore, the optical feature associated with absorption across the CDW gap persists well into the normal state.[81] The reason for this non-BCS behavior was explained by McMillan,[82] who pointed out that for sufficiently small coherence lengths, T_c is determined by the lattice entropy, rather than the entropy associated with particle-hole excitations across the gap. Thus, the transition is not of the "gap-opening" type, in contrast to BCS superconductors. By analogy, the small coherence length in the high-T_c cuprates may lead to a partial gap in the DOS above the transition temperature, although it is not clear what collective mode may play the role of phonons in CDW systems.

V. SUMMARY

In this paper we reported measurements and analysis of $\sigma(\omega, T)$ in crystals of $YBa_2Cu_3O_{6+x}$. In our analysis we emphasized the development of the spectral weight, and of features in σ, as the compounds change from insulator to high-T_c superconductor with varying O content or Al doping. In the following we summarize the main conclusions, beginning with the normal state.

A. Normal state

The essential first step in our analysis was to identify the free carrier and the interband contributions to σ. In metallic crystals σ, measured at 100 K, appears to contain at least two components, a narrow peak (with width $\sim 2k_B T$) centered at $\omega = 0$ and a broad component which extends to ≈ 2 eV. We associated the narrow peak with at least part of the free-carrier component because it extrapolates, as ω tends to zero, to values consistent with $\sigma_{dc}(T)$. We then examined the question of whether this peak accounts for the entire free-carrier contribution.

We concluded, for two reasons, that there is an additional contribution to σ from free carriers in the frequency range above the $\omega = 0$ peak, but below ≈ 1 eV. The first reason was that the spectral weight in the narrow peak N^*_{eff} is considerably less than is required to exhaust the f sum rule for the carrier density and band mass expected for our samples. [For example, $N^*_{eff} = 0.14$ in the 90-K superconductor, compared with a lower limit of 0.33 estimated from a carrier density of 0.33 holes per Cu(2) site, and a band mass equal to the electron mass.] The second reason was that there is a substantial component of spectral weight in the frequency range $k_B T < \omega < 0.5$ eV which increases rapidly with O concentration, and grows in proportion to the peak at $\omega = 0$. We estimated the spectral weight in this component, and found that it was consistent with the remainder of N_{eff} that we expected from the hole density and band mass.

Having identified, at least approximately, the free-carrier contribution to σ, we next analyzed its frequency dependence. The frequency dependence of the free-carrier conductivity is not "Drude-like," i.e., it cannot be described by a single Lorentzian peak centered at $\omega = 0$. The more complicated frequency dependence of σ suggests that the free carriers interact significantly with other excitations of the solid. In Secs. IV B and IV C, we attempted to extract from $\sigma(\omega, T)$ both the interaction strength and the distribution in energy of the excitations which scatter the carriers.

As a first step, we estimated the coupling strength from the relative weight of the two components of σ. We emphasized that, in the presence of interactions, $\sigma(\omega)$ is expected to separate into "coherent" and "incoherent" components at $T = 0$. The coherent component is the translational mode of the quasiparticle, and the ratio of the total free-carrier spectral weight to the weight in this mode defines the mass enhancement, which is a direct measure of the strength of the interaction. Unfortunately, in high-T_c compounds we cannot measure the normal state $\sigma(\omega)$ near $T = 0$, and consequently the identification of the coherent component is somewhat difficult. We estimated the spectral weight of this component by fitting $\sigma(\omega, 100\text{ K})$ at low frequency to a Lorentzian peak centered at $\omega = 0$. Although σ is still strongly T dependent at 100 K, these estimates are consistent with the analysis presented in Sec. IV C in which the coherent spectral weight is determined by fitting to a model in which the effects of nonzero T are included.

The coherent spectral weight N^*_{eff} was presented in Table I for each of the metallic samples. A mass enhancement $\approx 2-3$, follows from the ratio of the total weight to the coherent part. Collins *et al.*[83] obtained a similar value by fitting the optical conductivity of a $YBa_2Cu_3O_{6+x}$ crystal ($T_c \simeq 92$ K) with an inelastic scattering model. It is interesting that the interaction of holes with other excitations, as expressed through this mass enhancement, is not exceptionally strong. Similar mass enhancements are observed in Pb, Hg, and Nb_3Sn, for example, and attributed to electron-phonon coupling.[45] It should be remembered, however, that describing the carriers as holes absorbs into the carrier density the strong renormalization of the mass (due to short-range Coulomb repulsion), which leads to insulating behavior at half-filling.

In Sec. IV C we sought an $\alpha^2 F(\omega)$ consistent with the frequency and temperature dependence of the conductivity. We calculated $\sigma(\omega, T)$ for a model in which carriers

interact with a spectrum of dispersionless oscillators and compared the theoretical curves with experimental data. Surprisingly, we found that it was not possible to obtain a reasonable fit to the data in the temperature range 100–300 K and frequency range 20–4000 cm^{-1}. Although it was possible to fit σ at low frequency with a broad $\alpha^2F(\omega)$ and $\lambda=0.4$, the calculated curves were significantly smaller than the experimentally determined σ for $\omega>50$ meV. The extra conductivity cannot be accounted for by an additional contribution to $\alpha^2F(\omega)$ because this would create a deviation in the linearity of ρ_{dc} and Γ versus T, which is not observed. We were led by these observations to a two-component view of σ. At low frequency the translational mode of the quasiparticles is broadened by relatively weak coupling to low-energy excitations. Beginning at ~ 50 meV, there is another contribution to σ which accounts for the majority of the free-carrier spectral weight and cannot be explained by the usual inelastic scattering from a spectrum of Einstein modes. The onset of this contribution to σ becomes increasingly sharp as T is reduced and it is particularly distinct below T_c.

B. Superconducting state

In the discussion of the superconducting state we emphasized the appearance of two features in the reflectivity, which sharpen as the temperature is lowered. These features, which occur at ~ 150–200 cm^{-1} (18–24 meV) and at ~ 430 cm^{-1} (54 meV), correspond to thresholds in $\sigma(\omega)$. We compared the behavior of these thresholds with expectations for energy gaps associated with superconductivity.

Two properties of the higher-energy threshold are not well described in terms of a BCS gap: the threshold energy does not vary in crystals with different T_c's, and it is visible in the normal state $T>90$ K. The first property can be explained by sample inhomogeneity, if there is only one homogeneous superconductor with composition $YBa_2Cu_3O_{6+x}$, for which $x\simeq 0.9$ and $T_c=92$ K. The second property cannot be explained by inhomogeneity. In a recently reported study[57] of a crystal with $T_c=92$ K, the 50-meV feature was observed in the ratio $\sigma(\omega,105\ \text{K})/\sigma(\omega,150\ \text{K})$. This suggests that, in crystals with $T_c\simeq 90$ K (as well as reduced T_c samples), there is a structure in $\sigma(\omega)$ near 50 meV in the normal state.

The lower-energy threshold appears to be consistent with a conventional BCS gap. It is visible only in the superconducting state and varies with T_c in the $YBa_2Cu_3O_{6+x}$ crystals with reduced transition temperatures. We stated, however, that it is premature to associate this feature with a superconducting energy gap for several reasons: the absorption associated with this threshold is close to our detection limit, it is visible only in samples which have a high overall reflectivity, and its magnitude is small or unobservable in the crystals with $T_c=90$ K.

Next, we discussed the implications of recent experiments which probe, in different ways, the excitations of the cuprate superconductors in the same energy range as optical reflectivity. We emphasized the importance of direct probes of the one-particle DOS, such as tunneling and PE. PE spectra of $Bi_2Sr_2CaCu_2O_8$, which indicate a shift in the emission threshold at low energy and a pileup of intensity at threshold, strongly suggest the formation of a gap at low temperature. The value of Δ deduced from these measurements, ~ 30 meV, corresponds reasonably well to half the energy of threshold in $\sigma(\omega)$ at ≈ 400 cm^{-1}. This correspondence suggests that the optical structure results from particle-hole excitations across a gap at E_F, although more optical studies of $Bi_2Sr_2CaCu_2O_8$, and PE measurements in $YBa_2Cu_3O_{6+x}$ are needed to establish this identification. Finally, we described recent neutron scattering and NMR measurements, in which there are hints that the non-BCS behavior of the optical gap is mirrored in the spectrum of spin excitations.

A synthesis of optical, magnetic, and tunneling spectroscopies suggests that there is a relatively large gap at E_F related to electron pairing, but with properties are not well described by the BCS theory. We suggested an analogy to some layered metals with CDW ground states, in which a gap at E_F exists in the normal state, with an extremely large ratio of 2Δ to k_BT_c. A fascinating picture of the low-energy excitations of the cuprate superconductors is emerging; hopefully this picture will ultimately lead to a greater understanding of the physics which underlies the formation of the superconducting state at high temperature.

ACKNOWLEDGMENTS

We would like to thank P. B. Littlewood, S. Martin, and C. M. Varma for useful discussions, and we are grateful to B. Batlogg, S. H. Glarum, S. Martin, and L. W. Rupp, for help with characterization of samples and permission to use previously unpublished data. One of us (A.J.M.) thanks Patrick Lee for helpful conversations and the Aspen Center for Physics, where some of the work reported here was performed.

*Current address: Department of Physics, McMaster University, Hamilton, Ontario, Canada

[1]A. B. Pippard, in *Optical Properties and Electronic Structure of Metals and Alloys,* edited by F. Abeles (North-Holland, Amsterdam, 1966).

[2]T. Holstein, Ann. Phys. (N.Y.) **29**, 410 (1964).

[3]J. G. Bednorz and K. A. Müller, Z. Phys. B **64**, 189 (1986).

[4]N. P. Ong, Z. Z. Wang, J. Clayhold, J. M. Tarrascon, L. H. Greene, and W. R. McKinnon, Phys. Rev. B **35**, 8807 (1987).

[5]S. Uchida, H. Takagi, H. Ishii, H. Eisaki, T. Yabe, S. Tagima, and S. Tanaka, Jpn. J. Appl. Phys. Pt. 2 **26**, L445 (1987).

[6]For a review, see P. B. Allen, in *The Physical Properties of High Temperature Superconductors,* edited by D. M. Ginsberg (World Scientific, Singapore, 1989).

[7]P. W. Anderson, Science **235**, 1196 (1987).
[8]L. F. Schneemeyer, J. V. Waszczak, T. Siegrist, R. B. van Dover, L. W. Rupp, B. Batlogg, R. J. Cava, and D. W. Murphy, Nature (London) h**328**, 601 (1987).
[9]A. T. Fiory, S. Martin, L. F. Schneemeyer, R. M. Fleming, A. E. White, and J. V. Waszczak, Phys. Rev. B **38**, 7129 (1988).
[10]G. A. Thomas, M. Capizzi, T. Timusk, S. L. Cooper, J. Orenstein, D. H. Rapkine, S. Martin, L. F. Schneemeyer, and J. V. Waszczak, J. Opt. Soc. Am. B **6**, 415 (1989).
[11]T. Siegrist, L. F. Schneemeyer, J. V. Waszczak, N. P. Singh, R. L. Opila, B. Batlogg, L. W. Rupp, and D. W. Murphy, Phys. Rev. B **36**, 8365 (1987).
[12]L. W. Rupp and B. Batlogg (private communication).
[13]D. L. Rubin, K. Green, J. Gruschus, J. Kirchgessner, D. Moffat, H. Padamsee, J. Sears, Q. S. Shu, L. F. Schneemeyer, and J. V. Waszczak, Phys. Rev. B **38**, 6539 (1988).
[14]S. H. Glarum, S. H. Marshall, and L. F. Schneemeyer, Phys. Rev. B **37**, 7491 (1988); results on reduced T_c samples are unpublished.
[15]A. E. White (private communication); A. E. White, K. T. Short, J. P. Garno, J. M. Valles, R. C. Dynes, L. F. Schneemeyer, J. V. Waszczak, A. F. J. Levi, M. Anzlower, and K. W. Baldwin, Nucl. Instrum. Methods Phys. Res. B **37/38**, 923 (1989).
[16]R. M. Fleming, L. F. Schneemeyer, P. K. Gallagher, B. Batlogg, L. W. Rupp, and J. V. Waszczak, Phys. Rev. B **37**, 7920 (1988).
[17]C. H. Chen, D. J. Werder, L. F. Schneemeyer, P. K. Gallagher, and J. V. Waszczak, Phys. Rev. B **38**, 2888 (1988).
[18]S. H. Glarum, L. F. Schneemeyer, and J. V. Waszczak, Phys. Rev. B **41**, 1837 (1990).
[19]N. W. Ashcroft and N. D. Mermin, *Solid State Physics* (Holt, Rinehart, Philadelphia, 1976).
[20]F. Stern, *Solid State Physics* (Academic, New York, 1963), Vol. 15.
[21]S. Tajima, H. Ishii, T. Nakahashi, T. Takagi, S. Uchida, M. Seki, S. Suga, Y. Hidaka, M. Suzuki, T. Murakami, K. Oka, and H. Unoki, J. Opt. Soc. Am. B **6**, 475 (1989).
[22]J. Orenstein, G. A. Thomas, D. H. Rapkine, A. J. Millis, L. F. Schneemeyer, and J. V. Waszczak, Physica C **153-155**, 1740 (1988); G. A. Thomas, J. Orenstein, D. H. Rapkine, M. Capizzi, A. J. Jillis, R. N. Bhatt, L. F. Schneemeyer, and J. V. Waszczak, Phys. Rev. Lett. **61**, 1313 (1988); S. L. Cooper, G. A. Thomas, D. H. Rapkine, M. Capizzi, T. Timusk, A. J. Millis, L. F. Schneemeyer, and J. V. Waszczak, Phys. Rev. B **40**, 11 358 (1989).
[23]S. Tajima, T. Nakahashi, S. Uchida, S. Tanaka, M. Seki, and S. Suga, Physica C **156**, 90 (1988).
[24]M. Tinkham and R. A. Ferrell, Phys. Rev. Lett. **2**, 331 (1959).
[25]C. M. Varma, S. Schmitt-Rink, and E. Abrahams, Solid State Commun. **62**, 681 (1987).
[26]See H. Eskes and G. A. Sawatzky, Phys. Rev. Lett. **61**, 1415 (1988) for references to photoemission experiments.
[27]E. B. Stechel and D. R. Jennison, Phys. Rev. B **38**, 4632 (1988).
[28]A. K. McMahon, R. M. Martin, and S. Satpathy, Phys. Rev. B **38**, 6650 (1988).
[29]M. S. Hybertson, M. Schluter, and N. E. Christensen, Phys. Rev. B **39**, 9028 (1989).
[30]J. Zaanen, G. A. Sawatzky, and J. W. Allen, Phys. Rev. Lett. **55**, 418 (1985).
[31]L. F. Matheiss, Phys. Rev. Lett. **58**, 1028 (1987).
[32]J. Yu, A. J. Freeman, and J.-H. Xu, Phys. Rev. Lett. **58**, 1035 (1987).
[33]S. L. Cooper, G. A. Thomas, A. J. Millis, P. E. Sulewski, J. Orenstein, D. H. Rapkine, S-W. Cheong, and P. L. Trevor (unpublished).
[34]Z. Fisk (private communication).
[35]W. F. Brinkman and T. M. Rice, Phys. Rev. B **2**, 4302 (1970).
[36]S. Schmitt-Rink, C. M. Varma, and A. E. Ruckenstein, Phys. Rev. Lett. **60**, 2793 (1988).
[37]T. M. Rice and F. C. Zhang, Phys. Rev. B **39**, 815 (1989).
[38]C. L. Kane, P. A. Lee, and N. Read, Phys. Rev. B **39**, 6880 (1989).
[39]See, for example, *Proceedings of the International Conference on Materials and Mechanisms of Superconductivity,* edited by J. Muller and J. L. Olsen (North-Holland, Amsterdam, 1988).
[40]C. M. Varma, P. B. Littlewood, S. Schmitt-Rink, E. Abrahams, and A. E. Ruckenstein, Phys. Rev. Lett. **63**, 1996 (1989).
[41]J. Clayhold, S. Hagen, Z. Z. Wang, N. P. Ong, J. M. Tarrascon, and P. Barboux, Phys. Rev. B **39**, 777 (1989).
[42]A. J. Millis and S. N. Coppersmith (unpublished).
[43]J. Tanaka, K. Kamiya, and S. Tsurumi, Physica C **153-155**, 653 (1988).
[44]M. Suzuki, Phys. Rev. B **39**, 2312 (1989).
[45]See, for example, R. M. White and T. H. Geballe, *Long-Range Order in Solids* (Academic, New York, 1979).
[46]R. R. Joyce and P. L. Richards, Phys. Rev. Lett. **24**, 1007 (1970).
[47]P. B. Allen, Phys. Rev. B **3**, 305 (1971).
[48]A. B. Migdal, Zh. Eksp. Teor. Fiz. **34**, 1438 (1958) [Sov. Phys. JETP **7**, 996 (1958)].
[49]R. Kubo, in *Lectures in Theoretical Physics,* edited by W. E. Brittin (Wiley-Interscience, New York, 1957), Vol. I.
[50]B. Render, F. Gompf, E. Gering, G. Roth, W. Reichard, D. Ewart, and H. Rietschel, Physica C **153-155**, 272 (1988).
[51]J. H. Kim, K. Levin, R. Wentzcovich, and A. Auerbach, Phys. Rev. B **40**, 11 378 (1989).
[52]S. Martin, A. T. Fiory, R. M. Fleming, L. F. Schneemeyer, J. V. Waszczak, A. F. Hebard, and S. A. Sunshine, Phys. Rev. B **41**, 846 (1990).
[53]J. Bardeen, L. N. Cooper, and J. R. Schrieffer, Phys. Rev. **108**, 1175 (1957).
[54]Z. Schlesinger, R. T. Collins, D. L. Kaiser, and F. Holtzberg, Phys. Rev. Lett. **59**, 1959 (1987).
[55]G. A. Thomas, M. Capizzi, J. Orenstein, D. H. Rapkine, L. F. Schneemeyer, J. V. Waszczak, A. J. Millis, and R. N Bhatt, Jpn. J. Appl. Phys. Supp. **26**, 2044 (1987).
[56]T. Timusk, D. A. Bonn, J. E. Greedan, C. V. Stager, J. D. Garrett, A. H. O'Reilly, M. Reedyk, K. Kamaras, C. D. Porter, S. L. Herr, and D. B. Tanner, Physica C **153-155**, 1744 (1988).
[57]R. T. Collins, Z. Schlesinger, F. Holtzberg, and C. Feild, Phys. Rev. Lett. **63**, 422 (1989).
[58]J. Schützmann, W. Ose, J. Keller, K. F. Renk, B. Roas, L. Schultz, and G. Saemann-Ischenko, Europhys. Lett. **8**, 679 (1989).
[59]K. Kamaras, S. L. Herr, C. D. Porter, N. Tache, D. B. Tanner, S. Etemad, T. Venkatesan, and E. Chase, Phys. Rev. Lett. **64**, 84 (1990).
[60]T. Pham, H. D. Drew, S. H. Moseley, and J. Z. Liu (private communication).
[61]A. E. White, R. C. Dynes, and J. P. Garno, Phys. Rev. B **33**, 3549 (1986).
[62]For a review, see M. R. Beasley, Jpn. J. Appl. Phys. Suppl. **26**, 1967 (1987).
[63]M. Tinkham, *Introduction to Superconductivity* (McGraw-

Hill, New York, 1975).
[64]D. C. Mattis and J. Bardeen, Phys. Rev. **111**, 412 (1958).
[65]For a survey of ceramic materials, see Y. J. Uemora *et al.*, Phys. Rev. Lett. **62**, 2317 (1989); for recent results in a single crystal, see D. R. Harshman, L. F. Schneemeyer, J. V. Waszczak, G. Aeppli, R. J. Cava, B. Batlogg, L. W. Rupp, E. J. Ansaldo, and D. L. Williams, Phys. Rev. B **39**, 851 (1989).
[66]S. Martin (private communication).
[67]S. L. Cooper, F. Slakey, M. V. Klein, J. P. Rice, E. D. Bukowski, and D. M. Ginsberg, Phys. Rev. B **38**, 11 934 (1988).
[68]R. Hackl, W. Glaser, P. Muller, D. Einzel, and K. Andres, Phys. Rev. B **38**, 7133 (1988).
[69]J.-M. Imer, F. Patthey, B. Dardel, W.-D. Schneider, Y. Baer, Y. Petroff, and A. Zettl, Phys. Rev. Lett. **62**, 336 (1989).
[70]C. G. Olson, R. Liu, A.-B. Yang, D. W. Lynch, A. J. Arko, R. S. List, B. W. Veal, Y. C. Chiang, P. Z. Jiang, and A. P. Paulikas, Science **245**, 731 (1989).
[71]For a review, see M. Lee, A. Kapitulnik, and M. R. Beasley, in *Mechanisms of High Temperature Superconductivity,* edited by H. Kamimura and A. Oshiyama (Springer-Verlag, Heidelberg, 1989); for a more recent study, see M. Gurvitch, J. M. Valles, Jr., A. M. Cucolo, R. C. Dynes, J. P. Garno, L. F. Schneemeyer, and J. V. Waszczak, Phys. Rev. Lett. **63**, 1008 (1990).
[72]A. P. Volodin, B. Ya. Kotyuzhanskii, and G. A. Stepanyan, Pis'ma Zh. Eksp. Teor. Fiz. **48**, 457 (1988) [JETP Lett. **48**, 502 (1988)].
[73]J. S. Tsai, I. Takeuchi, J. Fujita, T. Yoshitake, S. Miura, S. Tanaka, T. Terashima, Y. Bando, K. Iijima, and K. Yamamoto, Physica C **153-155**, 1385 (1988).
[74]A. P. Fein, J. R. Kirtley, and M. W. Shafer, Phys. Rev. B **37**, 9738 (1988).
[75]M. Mali, D. Brinkmann, L. Pauli, J. Roos, H. Zimmermann, and J. Hulliger, Phys. Lett. A **124**, 112 (1987).
[76]W. W. Warren, Jr., R. E. Walstedt, G. F. Brennert, G. P. Espinosa, and J. P. Remeika, Phys. Rev. Lett. **59**, 1860 (1987).
[77]W. W. Warren, Jr., R. E. Walstedt, G. F. Brennert, R. J. Cava, R. Tycko, R. F. Bell, and G. Dabbagh, Phys. Rev. Lett. **62**, 1193 (1989).
[78]K. Yoshimura, T. Imai, Y. Ueda, and K. Kosuge, J. Phys. Soc. Jpn. **58**, 305 (1989).
[79]G. Shirane, R. J. Birgeneau, Y. Endoh, P. Gehring, M. A. Kastner, K. Kitazawa, H. Kojima, I. Tanaka, T. R. Thurston, and K. Yamada, Phys. Rev. Lett. **63**, 330 (1989).
[80]J. A. Wilson, F. J. DiSalvo, and F. Mahajan, Adv. Phys. **24**, 117 (1975).
[81]A. S. Barker, Jr., J. A. Ditzenberger, and F. J. DiSalvo, Phys. Rev. B **12**, 2049 (1975).
[82]W. L. McMillan, Phys. Rev. B **16**, 643 (1977).
[83]R. T. Collins, Z. Schlesinger, F. Holtzberg, P. Chaudhari, and C. Feild, Phys. Rev. B **39**, 6571 (1989).